


Network Pharmacology Analysis and Experimental Validation to Investigate the Mechanism of Total Flavonoids of Rhizoma Drynariae in Treating Rheumatoid Arthritis

Guang-yao Chen ^{1,*}, Jing Luo ^{2,3,*}, Yi Liu ^{4,*}, Xin-bo Yu ¹, Xiao-yu Liu ⁵, Qing-wen Tao^{2,3}

¹Graduate School, Beijing University of Chinese Medicine, Beijing, 100029, People's Republic of China; ²Department of TCM Rheumatology, China-Japan Friendship Hospital, Beijing, 100029, People's Republic of China; ³Beijing Key Lab for Immune-Mediated Inflammatory Diseases, China-Japan Friendship Hospital, Beijing, 100029, People's Republic of China; ⁴Humanities School, Beijing University of Chinese Medicine, Beijing, 100029, People's Republic of China; ⁵School of Traditional Chinese Medicine, Beijing University of Chinese Medicine, Beijing, 100029, People's Republic of China

*These authors contributed equally to this work

Correspondence: Qing-wen Tao, Department of TCM Rheumatology, China-Japan Friendship Hospital, Beijing, People's Republic of China, Tel +8613910528490, Email taoqgl@outlook.com

Objective: The study aimed to explore the mechanism of total flavonoids of Rhizoma Drynariae (TFRD) in the treatment of rheumatoid arthritis (RA) based on network pharmacology and experimental validation.

Methods: The active components of TFRD were identified from TCMSp and TCMID databases. Relevant targets of the active compounds of TFRD and RA-related targets were predicted by public databases online. A component-target (C-T) regulatory network was constructed by Cytoscape. The genes of TFRD regulating RA were imported into STRING database to construct a protein-protein interaction (PPI) network in order to predict the key targets. KEGG enrichment analysis was performed to predict the crucial mechanism of TFRD against RA. The active components of TFRD underwent molecular docking with the key proteins. Collagen-induced arthritis (CIA) model of rats and inflammatory factors-stimulated fibroblast-like synoviocytes were used in vivo and in vitro to validate the efficacy and predicted critical mechanisms of TFRD.

Results: Network Pharmacology analysis revealed that TFRD had 14 active compounds, corresponding to 213 targets, and RA related to 2814 genes. There were 137 intersection genes between TFRD and RA. KEGG indicated that therapeutic effects of TFRD on RA involves T cell receptor signaling pathway, Th17 cell differentiation, IL-17 signaling pathway, TNF signaling pathway, MAPK signaling pathway and PI3K/AKT signaling pathway. In vivo experiments suggested TFRD can alleviate the inflammatory response, joint swelling and synovial abnormality of CIA rats. TFRD contributed to the decrease of Th17 cells and the down-regulated secretion of IL-17A and TNF- α of activated lymphocyte in CIA model. In vitro experiments confirmed TFRD can effectively inhibit the inflammatory response of fibroblast-like synoviocytes and suppress the abnormal activation of MAPK, PI3K/AKT and NF κ B signaling pathways.

Conclusion: The treatment of RA with TFRD is closely related to inhibiting Th17 differentiation and inflammatory response of synoviocytes.

Keywords: total flavonoids of Rhizoma Drynariae, Rheumatoid arthritis, network pharmacology, T cell differentiation, inflammatory response

Introduction

Rheumatoid arthritis (RA) is a chronic autoimmune disease that characteristically presents as symmetrical peripheral polyarthritis, whose prevalence is approximately 0.5–1% in worldwide.¹ Although the specific pathogenesis of RA has not been completely elucidated, relevant evidence shows that the occurrence of RA is related to infection, genetic, environmental

and other potential factors.²⁻⁴ The pathologic manifestations of RA are mainly inflammatory response and abnormal hyperplasia of joint synovium, accompanied by the formation of synovial microvasculature.⁵ If the inflammatory response of RA is poorly controlled, the invasion of synovial tissues can cause bone erosions and cartilage destruction, ultimately resulting in joint deformity.⁶

Currently, disease-modifying anti-rheumatic drugs (DMARDs) are the most commonly used drug for RA in clinic practices, including conventional synthetic DMARDs (csDMARDs), biologic DMARDs (bDMARDs) and targeted synthetic DMARDs (tsDMARDs).⁷ Methotrexate, the representative of csDMARDs, is a cornerstone of treatment for RA; however, its clinical application is limited by slow onset and serious side-effects such as myelosuppression, nephrotoxicity and hepatotoxicity.⁸ Biologic DMARDs (bDMARDs) and targeted synthetic DMARDs (tsDMARDs) have a prompt and excellent effect on inhibiting inflammatory response, but potential risk of infections still exists.⁹⁻¹¹ Therefore, it is urgently necessary to discover more effective and safer drugs for treatment of RA.

Traditional Chinese Medicine (TCM) have been used for the treatment of RA in China for thousands of years. The earliest formulas (*Wutou* decoction and *GuiZhi-ShaoYao-ZhiMu* decoction) for treatment of RA were recorded in the *Synopsis of Prescriptions of the Golden Chamber* written 2000 years ago. The treatment of RA with TCM has a definite curative effect and few side-effects, and can provide individualized therapy according to the clinical characteristics of each patient.^{12,13} Tripterygium glycosides, total glucosides of paeony and sinomenine, extracts of TCM herbs, have been proven to have good therapeutic effects on RA by randomized controlled trials (RCTs), and are recommended to be applied to the clinical treatment of RA by Chinese current clinical guidelines.¹⁴⁻¹⁶

Rhizoma Drynariae, the dried rhizome of *Drynaria roosii* Nakaike [Polypodiaceae], has the effect of tonifying kidney and strengthening the function of bone, and is widely applied to treat rheumatic diseases. Flavonoid compounds are the main active components in Rhizoma Drynariae, and total flavonoids of Rhizoma Drynariae (TFRD) are approved by Chinese Nation Medicine Products Administration for the clinical treatment of osteoporosis. Osteoporosis usually occurs in patients with RA.¹⁷ Clinical studies revealed that TFRD can not only effectively improve osteoporosis, but also alleviates joint swelling, tenderness and morning stiffness symptomatic of RA.¹⁸ Meanwhile, inflammation-related indicators, including erythrocyte sedimentation rate (ESR) and C-reactive protein (CRP) show a remarkable decrease after treatment with TFRD, which indicated TFRD has potential therapeutic effects on RA.¹⁸ In the study, in order to investigate the precise mechanism of the treatment of RA with TFRD, the core targets and mechanism of TFRD in treating RA were predicted by Network Pharmacology, and then validated by in vivo and in vitro experiments (Figure 1).

Materials and Methods

Prediction of Active Compounds of TFRD

The compounds of Rhizoma Drynariae were acquired by searching the Traditional Chinese Medicine Systems Pharmacology Database and Analysis Platform (TCMSP) (<http://tcmsp.com>)¹⁹ and Traditional Chinese Medicine Integrated Database (TCMID) (<http://47.100.169.139/tcmid>).²⁰ Flavonoids of Rhizoma Drynariae were screened in accordance with molecular structure, among which the key compounds were screened using the method described below.

First, active flavonoids were identified on the basis of absorption, distribution, metabolism and excretion (ADME). Flavonoids acquired from TCMSP database were screened based on the criteria of Oral Bioavailability (OB) $\geq 30\%$ and drug-like (DL) ≥ 0.18 . If the component cannot be retrieved from TCMSP, Lipinski rule of five was used to determine whether the compound was included in the research. Second, a systematic literature search for flavonoids of Rhizoma Drynariae was conducted, and subsequently flavonoids whose therapeutic efficacy on RA was confirmed by previous studies were included in the research.^{21,22}

Validation of Active Compounds of TFRD

The sample of TFRD was prepared by macroporous adsorption resin in our previous experiments.²³ The prepared sample was detected by a liquid chromatograph coupled to a mass spectrometer (LC-MS) to recognize whether the predicted active ingredients were available in the sample used for subsequent experiments. The specific process is described below.

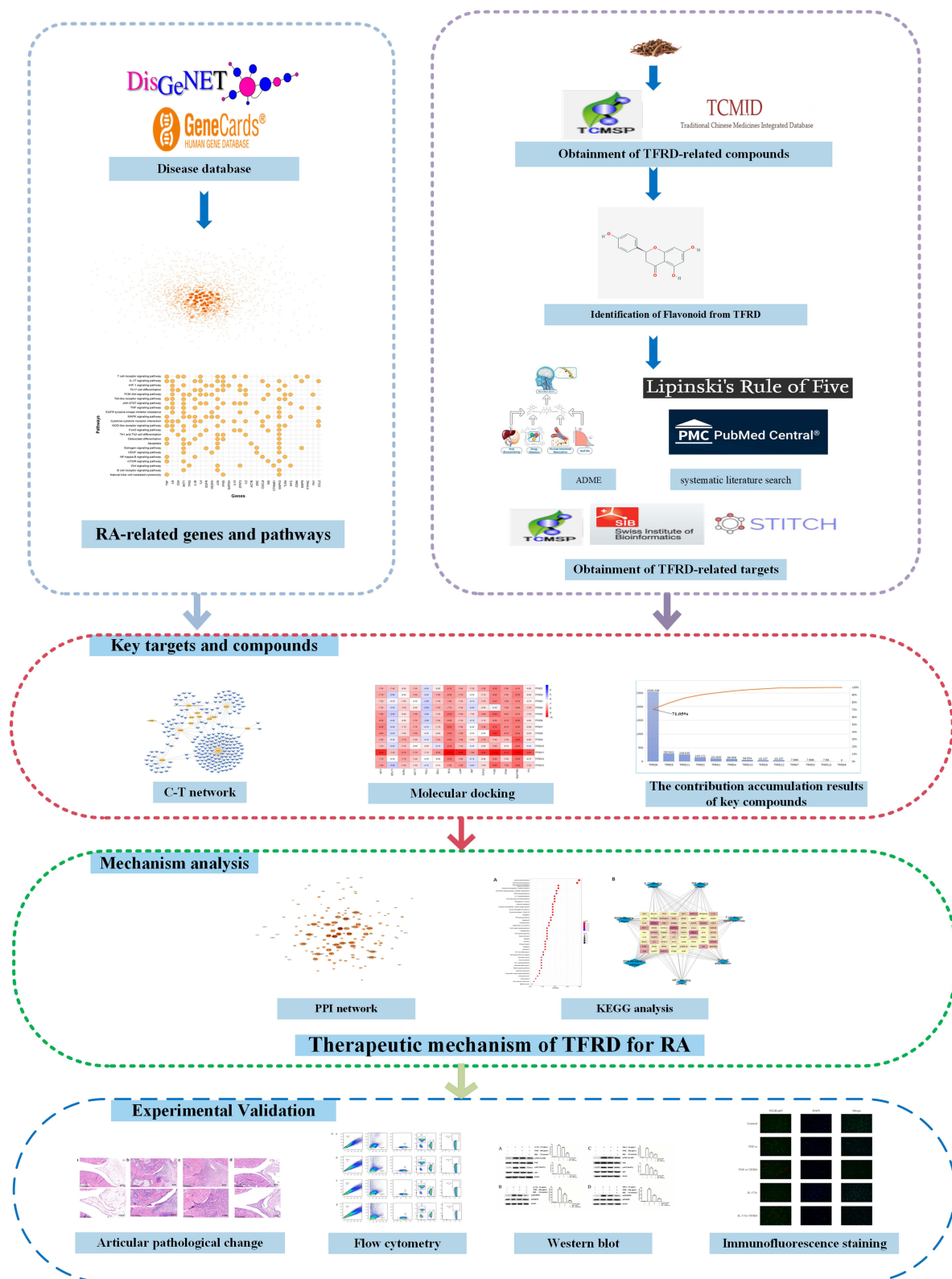


Figure 1 The flowchart of this study. Network pharmacology approach includes the acquirement of RA-related genes and TFRD-related compounds and targets, construction of C-T network, accumulation of key compounds, PPI network construction, KEGG enrichment analysis, molecular docking. Experimental validation involves pathological images, flow cytometry, Western blotting, immunofluorescence.

Abbreviations: RA, Rheumatoid arthritis; TFRD, total flavonoid of Rhizoma Drynariae.

20 mg of TFRD sample was added to 1 mL of deionized water for ultrasound for 30 min and centrifuged at 12,000 r/min for 10 min to obtain supernatant. The supernatant was filtered by a 0.22 μm membrane for sample detection. The TFRD was detected by a Nexera High-Performance Liquid Chromatograph (Japan Shimadzu Co., Ltd) coupled to a SCIEX 5600 Triple-TOF Mass Spectrometer (Sciex, Toront, Canada). Chromatography separation was carried out on HSS T3 C18 analytical column (100 mm \times 2.1 mm, 1.8 μm). The mobile phase consisted of 0.1% formic acid/99.9 H₂O (A) and 99.9% acetonitrile/0.1% formic acid (B), and run under the following program: 0–5 min, 15%–15% B; 5–13 min, 15%–16% B; 13–17 min, 16%–16% B; 17–20 min, 16%–17% B; 20–26 min, 11%–95% B, 26–27 min 95%–15% B, 27–30 min, 15%–15% B. The flow rate was set at 0.3 mL/min. The results were compared with MassBank online Spectral Database (<https://massbank.eu/MassBank/>), The ReSpec DB (<http://spectra.psc.riken.jp>) and GNPS platform (<https://gnps.ucsd.edu/>).

The Targets of Active Compounds of TFRD

Potential targets of active compounds of TFRD were derived from TCMSP database, SwissTargetPrediction database and STITCH database. Potential targets were obtained from TCMSP and then their abbreviations were standardized by Unitprot database. Meanwhile, PubChem database was employed to establish the canonical SMILE of active compounds. The prediction of targets was performed using the SwissTargetPrediction database and STITCH database, and then targets satisfying the criterion of Confidence >0.4 were included in the subsequent study.^{24,25} The targets corresponding to the active components of TFRD predicted by the above two approaches were combined and used for further study.

Prediction of RA-Related Targets

“Rheumatoid Arthritis” was used as the keyword to obtain RA-related genes from GeneCards and DisGeNET databases. The screening conditions were set at GeneCards’ Score ≥ 0.05 and DisGeNET’s Score ≥ 0.1 .^{26,27} After overlapping genes acquired from the above two databases were removed, the rest were considered as RA-genes of the study. A Venn diagram was generated by R language software to identify the intersection targets of RA and TFRD, defined as the targets of TFRD regulating RA.

Construction of C-T Network and Prediction of Key Targets

Active compounds, the targets of active compounds and targets of TFRD regulating RA were utilized to establish compounds-targets (C-T) network by Cytoscape (Version 3.8.2).

Meanwhile, mathematical models were created to obtain the degree of the contribution of active compounds and targets to C-T network for the purpose of screening the most key targets.

Pathway Enrichment Analysis

The signaling pathways involved in the genes were analyzed by KEGG enrichment analysis. KEGG enrichment analysis was performed by clusterProfiler package in R software. The signaling pathways of $P < 0.05$ were determined as key pathways. In order to obtain the key signaling pathways of RA, the first 30% of RA-related genes derived from GeneCards and DisGeNET databases were aggregated. These genes were input into the STRING database to generate a protein-protein Interaction (PPI) network. The 30 genes with the greatest contributions to the PPI network were considered as key genes and subjected to KEGG analysis to determine the key pathways of RA. At the same time, the KEGG pathway enrichment analysis was also performed on the intersection genes between RA and active compounds of TFRD to identify the important pathways that may be regulated by the active components of TFRD in treating RA.

Prediction of Key Components of TFRD

The key components of TFRD were obtained by the two methods described below. The degree of contribution of each of the active compounds was calculated to determine the importance of active components in the network. A regulatory network of Optimization Space was built on the basis of the C-T network and genes in the PPI network of RA. Subsequently, the degree of contribution of each active compound was calculated in accordance with the number of targets connecting with each compound in the C-T network and connection combined score of each gene in the PPI network. The calculation procedure can be described as follows:

We defined $Net = \{N, E\}$. In this formula, N denotes the Matrix of Nodes and E denotes the Matrix of Nodes Edge. Namely, the PPI network of RA, the C-T network of active compounds is $Net_{compound} = \{N_{compound}, E_{compound}\}$. An optimal space network is $Net_{OS} = \{N_{CT}, E_{OS}\}$. If $Net_{OS} = Net_{disease} \cup Net_{compound}$, it is easy to have too many redundant connections, so we only include the part of Net where the degree is greater than the average, i.e.

$$Net_{OS} = Net_{disease} \cup Net_{compound}(degree > \overline{degree})$$

Then, the degrees of the compounds in Net_{OS} are sorted in descending order and the Cumulative Frequencies (CF) are calculated to obtain the core compounds. Set the degree of the k th compound to d_k , and $d_1 > d_2 > \dots > d_k > \dots > d_n$, then the Cumulative Frequency of the k_{th} compound is as follows:

$$CF(k) = \frac{\sum_{i=1}^k d_i}{\sum_{i=1}^n d_i}, (k = 1, 2, \dots, n)$$

If $CF(k) > 0.5$, $compound_{1\sim}$ are considered as the key compounds in quality controls of the herb.

Molecular docking was performed to identify the key compound of TFRD according to binding energy between active compounds of TFRD and key proteins of signaling pathways predicted by KEGG enrichment analysis. The three-dimensional structures of the key proteins were downloaded from the RCSB PDB database. The structures of the key compounds of TFRD were downloaded from TCMSP database, and were saved as MOL2 format. Autodock Vina was utilized to conduct molecular docking. A heat map was generated with assistance of the R language “heat map” function to visualize the values of the binding energy of molecular docking and was used as the basis for obtaining the key components of TFRD.^{28–30} The lower the value is, the higher the affinity is and the stronger the interaction between a target and a protein is.

Experimental Validation

Reagents and Antibodies

Immunization grade bovine type II collagen (20022, Chondrex, USA), Incomplete Freund's adjuvant (7002, Chondrex, USA), EDTA- Na_2 (E8030, Solarbio, China), Phorbol 12-myristate 13-acetate (PMA) (P1585, Sigma-Aldrich, USA), Ionomycin Calcium Salt (I8800, Solarbio, China), DMEM Medium (C11995500BT, Gibco, USA), Penicillin-Streptomycin (V900929, Sigma-Aldrich, USA), Fetal Bovine Serum (FBS) (10099-141, Gibco, USA), Recombinant Human TNF- α (300-01A, Peprotech, USA), Recombinant Human IL-17A (200-17, Peprotech, USA), Electrochemiluminescence (ECL) luminous fluid (WBKLS0100, Millipore, USA), Polyvinylidene difluoride (PVDF) membranes (ISEQ00010, Millipore, USA), Animal-free Blocking Solution (15019S, Cell Signaling, USA), RIPA lysis buffer (R0010, Solarbio, China), Phenylmethanesulfonyl fluoride (PMSF) (P0010, Solarbio, China), Leukocyte activation cocktail with GolgiPlug (552843, BD, USA).

CellTiter 96[®] Aqueous One Solution Cell Proliferation Assay (G358A, Promega, USA), Reverse Transcription System (A3500, Promega, USA), HiPure Total RNA Mini Kit (R4111-02, Magen, China), 10% PAGE Gel Fast Preparation Kit (PG112, EpiZyme, China), Nuclear Extraction Kit (SN0020, Solarbio, China), C-reactive protein Assay Kit (E023-1-1, NanJing JianCheng Bioengineering Institute, China), Hematoxylin-Eosin/HE Staining Kit (G1120, Solarbio, China), Human IL-6 enzyme-linked immunosorbent assay (ELISA) kits (CHE0009, Beijing 4A Biotech, China), Human TNF- α ELISA kits (CHE0019, Beijing 4A Biotech, China).

Anti-CD3-BV605 (563949, BD, USA), anti-CD4-BV711 (743092, BD, USA), anti-CD8a-PERCP (558824, BD, USA), anti-CD68-FITC (562117, BD, USA), anti-CD90-APC (328113, Biolegend, USA), anti-IL-17A-PE-CY7 (25-7177-82, eBioscience, USA) antibody, Vimentin antibody (PE Conjugate) (12020S, Cell Signaling, USA), Vimentin antibody (A19607, Abclonal, China), AKT antibody (4691S, Cell Signaling, USA), p-AKT (S473) antibody (4060S, Cell Signaling, USA), NF- κ B p65 (8242T, Cell Signaling, USA), I κ B- α antibody (4814T, Cell Signaling, USA), PI3K antibody (A4992, Abclonal, China), p38 MAPK antibody (A14401, Abclonal, China), p-p38 MAPK antibody (AP0526, Abclonal, China), Lamin B1 antibody (YT5180, Immunoway, USA), p-PI3K (Y467/199) antibody (YP0224, Immunoway, USA), β -Actin antibody (TA-09, Zhongshan Jingqiao Biotechnology, China), horseradish peroxidase (HRP)-conjugated goat anti-mouse IgG (ZB-5305, Zhongshan Jingqiao Biotechnology, China), HRP-conjugated goat anti-rabbit IgG (ZB-2301) and Alexa Fluor 488-conjugated Goat anti-Rabbit IgG (H+L) (ZF-0511, Zhongshan Jingqiao Biotechnology, China).

Animal Breeding

Male Sprague-Dawley rats (6 weeks, 200±10g) were purchased from Sibeifu Biotechnology Co., Ltd. The animal experimental protocol was approved by the experimental animal care and welfare ethics committee of China-Japan Friendship Hospital (No: zryhyy-21-21-05-07). Rats were housed in an animal room of China-Japan Friendship Hospital, whose environment is in complete accordance with Laboratory Animal-Requirements of Environment and Housing Facilities (GB 14925-2010, National Laboratory Animal Standardization Technical Committee of China). Prior to the experiments, rats were acclimatized to the breeding environment for 1 week to eliminate stress.

Establishment of the CIA Models and Pharmacologic Interventions

The process of the establishment of the CIA models by the injection of Type II collagen and incomplete Freund's adjuvant into the root of the tail. The specific process was as follows: 1 mL of incomplete Freund's adjuvant was added into a plastic test tube and then homogenized in an ice water bath while 1 mL of bovine type II collagen was added dropwise to the test tube until a milky drop is added to the water without spreading. The homogenized collagen was wrapped in tinfoil and then ready for injection. The tail of each rat was wiped with alcohol cotton balls to expose the skin near the root of the tail. 0.2 mL of collagen was subcutaneously injected into the left side of the tail root of each rat. The injection was repeated one week later with 0.1 mL of collagen in the same way.

The clinical daily dose of TFRD for osteoporotic patients is 750 mg. The dosage was calculated according to an individual's body weight for an adult at 60 kg; therefore, the daily dose for an adult is 12.5 mg/kg. According to the ratio of rat to human body surface area, the daily dose for rats is 6.3 times of an adult, and hence, the daily dosage of rats was 78.75 mg/kg. TFRD powder was prepared into 7.875 mg/mL solution with normal saline, and the solution was stored in a refrigerator at 4°C until use. RA patients were usually treated weekly with 10 mg MTX in clinical application, so the dosage of rats was 1.05 mg/kg once a week. MTX was dissolved into solution with normal saline (0.105 mg/mL final concentration), and the solution was stored at 4°C until use.

Using a random digit table method, 48 rats were randomly divided into four groups: normal group, CIA model group, TFRD group and MTX group. The CIA model group, TFRD group and MTX group were used to establish the CIA rat model. The TFRD group and MTX group were given a gavage of TFRD and MTX respectively at 8:00 AM for 2 weeks before modeling, and gavage ended by 3 weeks after the second injection of bovine type II collagen (the total intervention lasted six weeks). The normal group and CIA model group were fed with the same volume of normal saline.

Sample Processing

After intervention ended, the rats were anesthetized with 3.5% isoflurane/oxygen mixture and subsequently maintained with 1.5–2% isoflurane/oxygen mixture in an anesthetic chamber using a volume ventilator. Blood samples were obtained from the abdominal aorta and collected into sterile sodium heparin-containing tubes. 3 mL of blood samples were centrifuged to obtain the supernatant for detection of CRP contents. 200 µL of blood was subjected to flow cytometry to determine the proportion of Th17 cells. The rest of the blood samples were used to isolate lymphocytes to detect the expression of TNF- α and IL-17A after lymphocytes were activated.

Rat ankle joints were separated with bone forceps and muscle tissue was removed as much as possible. After rinsing with PBS, ankle joints were fixed with 4% paraformaldehyde for 72 h. Ankle joints were decalcified in 10% EDTA-Na₂ for 8 weeks and the decalcification solution was replaced once a week.

Assessment of Joint Swelling and Synovial Pathology

Swelling grade of joints was evaluated by two graders on the basis of a semi-quantitative score (0–4) (Table 1) without knowledge of the grouping and drug administration of the rats.³¹ The score for each rat was the sum of scores of both legs, and the final score was the average of two investigators' scores. The decalcified ankle joints were sequentially subject to embedding, slicing, dewaxing, HE staining and observed under a light microscope.

Cell Culture and Authentication

Fibroblast-like synoviocytes from RA patients (RA-FLSs) were isolated from the discarded synovial tissue of RA patients subjected to knee replacement, which was approved by Ethics Committee of China-Japan Friendship Hospital

Table 1 Scale of Joint Swelling of Rats

Score	Degree
0	Normal paw and no inflammation
1	Slight swelling/redness of metatarsophalangeal joint
2	Swelling/redness of metatarsophalangeal joint and toe
3	Swelling/redness of the foot below the ankle joint
4	Severe redness and swelling of ankle and signs of joint deformation

(No. 2021-153-K111). The obtained synovial tissue was soaked in sterile PBS and brought to the ultra-clean table. The synovial tissue was soaked with 75% alcohol to sterilize for 1 min, followed by three times washing with PBS containing penicillin and streptomycin. Then, the tissue was cut into 1 mm³ pieces and then digested with 0.25% trypsin for 20 min. DMEM complete medium (89% DMEM basic medium, 10% FBS and 1% penicillin/streptomycin) was used to neutralize trypsin. The synovial tissue was subjected to the digestion of 0.1% collagenase type II for 4 h and filtering with a 100 µm mesh screen. The filtered liquid was finally collected and centrifuged. Plenty of RA-FLSs were available in the centrifuged precipitation. RA-FLSs were cultured in DMEM complete medium, and placed in a humidified incubator with 5% CO₂ at 37°C. SW982 cells given by Professor Cheng Xiao from the China-Japan Friendship Hospital were cultured in the airtight medium containing L-15 complete medium (89% L-15 basic medium, 10% FBS and 1% penicillin/streptomycin) inside the incubator at 37°C. When the culture flask was covered with cells, the cells were digested with 0.25% trypsin and subcultured with a 1:2 ratio. Immunofluorescence and flow cytometry were used to identify the cell markers and the purity of RA-FLS.

Pharmacologic Intervention for Cells

The effects of TFRD on RA-FLS cell proliferation were detected by the MTS method so as to determine the maximum concentration of TFRD for intervention. 5000 cells were planted with 100 µl complete medium on a 96-well plate, and then TFRD at different concentrations was added for intervention. After a 24 h culture, the medium was discarded, and cells were washed with PBS twice. Then, 100 µL DMEM basic medium was added and incubated for 4 h. 20 µL MTS solution was added followed by incubation for 1 h, and the absorbance at 490 nm was recorded on a microplate reader. The maximum concentration of TFRD that did not affect cell proliferation was deemed the maximum intervention concentration for the subsequent experimental intervention. 100nmol/mL dexamethasone (DEX) was used as positive control drug.

500,000 cells were seeded in 6-well plates and pretreated with TFRD for 1 h. Then, pro-inflammatory cytokines (10 ng/mL of IL-17A or 10 ng/mL of TNF-α) were added as inflammatory stimulation. After intervened by corresponding drugs, the medium was collected and centrifuged, and the supernatants were collected for ELISA. The cells were lysed to be used for Western blot and real time-PCR (RT-PCR).

RT-PCR

After intervention, RA-FLSs were washed with PBS twice. Total RNA was isolated using HiPure Total RNA Mini Kit strictly based on the manufacturer's instructions. 1 µg total RNA was used for reverse transcription with Reverse Transcription System (Promega) to obtain cDNA according to the manufacturer's instructions. A 20 µL of reaction system included SYBR Green real-time PCR master mix, cDNA, forward primers and reverse primers was used for cDNA amplification following the manufacturer's instruction, and Ct values for each gene was calculated. The relative amount of target gene expression was calculated by the 2^{-ΔΔCt} method.

Western Blot

After intervention, RA-FLSs were washed with PBS twice. Cells were lysed by RIPA buffer (containing 1% PMSF and 1% phosphatase inhibitors) on ice for 30 min. After BCA assay was performed to detect total protein concentration, cell lysate was boiled with 5 × loading buffer. 10% SDS-PAGE gel was configured by a PAGE Gel Fast Preparation Kit base on the manufacturer's instructions. After prepared samples were centrifuged, 40 µg proteins were subjected to SDS-

polyacrylamide gel electrophoresis (SDS-PAGE), and then proteins were transferred at 70 V to a PVDF membrane from SDS-PAGE gel. The PVDF membranes were blocked in 5% nonfat milk/TBST for 1 h and incubated with primary antibody solutions overnight at 4°C. The membranes were washed with TBST five times; then, HRP-conjugated secondary antibody was added. Signals were detected by chemiluminescence using ECL luminous fluid and gray values were detected by Image J software.

ELISA and Immunonephelometry

Lymphocytes were separated from blood of rats with lymphocyte separation solution. The density of lymphocytes was quantified via a hemacytometer, and then lymphocytes were resuspended in RPMI 1640 complete medium and diluted to 1×10^6 cells/mL. After PMA (50ng/mL) and Ionomycin (1 μ g/mL) were added into the suspensions, lymphocytes were incubated for 6 h in an incubator at 37 °C. After centrifugation, the supernatant was subjected to ELISA assay according to the manufacturer's instructions.

The optical density (OD) of each well was measured by a microplate reader at a wavelength of 450 nm, with 650 nm the reference wavelength. The standard curve of concentration of the standard sample and the corresponding OD values were fitted by CurveExpert V1.4 software, and the sample concentration of each well was calculated by standard curve formula. CRP in the plasma was assessed using the immunoturbidimetric method in accordance with the manufacturer's instructions. The OD value of each well was measured by a microplate reader at a wavelength of 600 nm. The concentrations of standard sample and the corresponding OD values were fitted to a curve by Curve expert 1.4 and used as a reference to calculate the concentration for each sample well.

Immunofluorescence

Immunofluorescence was conducted to detect Vimentin and NF κ B p65 of RA-FLSs. Culture medium was discarded, cells were washed with PBS, fixed with 4% paraformaldehyde for 15 min, and permeabilized with 0.1% Triton. After one hour of blockage with 1 \times Animal Free Blocking Solution at room temperature, primary antibodies (anti-Vimentin at 1:100 dilution and anti-NF κ B at 1:200 dilution) were added into plate at 4°C overnight. Primary antibodies were discarded, Alexa Fluor 488-conjugated Goat anti-Rabbit IgG (H+L) (1:50 dilution) was added into plate and incubated at room temperature for 1 h. After secondary antibodies were discarded, fluorescent mounting medium with DAPI was added into plate and observations were performed using a fluorescent microscope (Zeiss).

Flow Cytometry

Detecting the proportion of Th17 cells in the lymphocytes was performed as described below. 200 μ L of blood samples and 200 μ L of RPMI 1640 complete medium were blended with leukocyte activation cocktail and incubated for 6 h. Subsequently, CD3 and CD8 antibodies were added into the samples and incubated for 15 min. After lysis of erythrocytes and fixation and permeabilization of the remaining cells, IL-17A antibody was added into samples and incubated for 30 min and then measured by flow cytometry.

The process to detect the markers of RA-FLSs was described below. RA-FLSs and SW982 cells were digested with EDTA-free Trypsin. CD90 antibodies were added into the samples and incubated for 15 min. After fixation and permeabilization, Vimentin and CD68 antibodies were added into samples, incubated for 30 min and then measured by flow cytometry.

Data Analysis

Continuous variables were presented as the mean values \pm standard deviation (SD). If data showed a normal distribution, Student's *t*-test was used to assess the differences between the two groups; if not, the Mann–Whitney test was utilized. ANOVA and the Dunnett's test were used for comparisons of multiple groups. P-value <0.05 was considered to indicate a statistically significant difference.

Results

Active Compounds of TFRD

By searching the databases, 71 compounds of *Rhizoma Drynariae* were obtained from TCMSP and 53 compounds of *Rhizoma Drynariae* were derived from TCMID. A total of 113 compounds were acquired after eliminating the common compounds. 51 flavonoids were identified based on molecular structure. 10 effective flavonoids were ultimately screened out on the basis of ADME, including (2R)-5,7-dihydroxy-2-(4-hydroxyphenyl) chroman-4-one (TFRD1), Aureusidin (TFRD2), Eriodyctiol (flavanone) (TFRD3), kaempferol (TFRD4), naringenin (TFRD5), (+)-catechin (TFRD6), eriodictyol (TFRD7), luteolin (TFRD8), davallioside A_{qt} (TFRD9) and xanthogalenol (TFRD10). Also, hesperidin (TFRD11),^{32,33} kurarinone (TFRD12)³⁴ and astragalín (TFRD13),³⁵ effective flavonoids identified from a comprehensive literature research, have been found to have demonstrated beneficial effects on rheumatoid arthritis. The 13 key compounds information including molecule name, molecular formula, molecular weight, OB and DL are shown in Table 2.

Identification of Active Compounds of TFRD with UHPLC-MS

Identification of active compounds of TFRD was performed using LC-MS, whose results showed that all 13 active compounds were available in the sample of TFRD (Figure 2). The LC-MS detailed information of 13 active compounds are shown in Table 3.

Core Genes and Key Pathways of RA

5020 genes related to RA were acquired from the GeneCards, 2725 genes related to RA from the DisGeNET database. After removing overlapping targets, 5861 RA-related genes were determined. We used the top 30% as the criteria in the selection of databases. 816 and 1504 RA-related genes were screened out from DisGeNET database and GeneCards database, respectively. 1795 genes were obtained after deleting the duplicate genes. A total of 1616 genes were engaged in the PPI network of RA (Figure 3A), which engaged 60,847 connections, and calculated combined score of each connection. The 30 genes of maximum connections were used to KEGG enrichment analysis, and thus 151 pathways with $P < 0.05$ were identified. After a systematic literature search was performed, 23 pathways closely related to RA were selected, which were utilized to construct the connection graph between core genes and key pathways (Figure 3B).

Construction of Compound-Target Network

A total of 266 targets corresponding to the 13 active ingredients of TFRD were obtained from TCMSP, SwissTargetPrediction and the STITCH databases, and 213 targets were obtained after the removal of common targets. 154 intersection genes between RA and TFRD were obtained and then defined as the targets of TFRD in the treatment of

Table 2 Detail Information of 13 Key Compounds

Molecule ID	Molecule Name	OB(%)	DL	MW	Chemical Formula
TFRD1	(2R)-5,7-dihydroxy-2-(4-hydroxyphenyl) chroman-4-one	42.36	0.21	272.27	C ₁₅ H ₁₂ O ₅
TFRD2	Aureusidin	53.42	0.24	286.25	C ₁₅ H ₁₀ O ₆
TFRD3	Eriodyctiol (flavanone)	41.35	0.24	288.27	C ₁₅ H ₁₂ O ₆
TFRD4	Kaempferol	41.88	0.24	286.25	C ₁₅ H ₁₀ O ₆
TFRD5	Naringenin	59.29	0.21	272.27	C ₁₅ H ₁₂ O ₅
TFRD6	(+)-catechin	54.83	0.24	290.29	C ₁₅ H ₁₄ O ₆
TFRD7	Eriodyctyol	71.79	0.24	288.27	C ₁₅ H ₁₂ O ₆
TFRD8	Luteolin	36.16	0.25	286.25	C ₁₅ H ₁₀ O ₆
TFRD9	Davallioside A _{qt}	62.65	0.51	373.39	C ₁₉ H ₁₉ NO ₁₂
TFRD10	Xanthogalenol	41.08	0.32	354.43	C ₂₁ H ₂₂ O ₅
TFRD11	Hesperidin	13.33	0.67	610.62	C ₂₈ H ₃₄ O ₁₅
TFRD12	Kurarinone	29.23	0.64	438.56	C ₂₆ H ₃₀ O ₆
TFRD13	Astragalín	14.03	0.74	448.41	C ₂₁ H ₂₀ O ₁₁

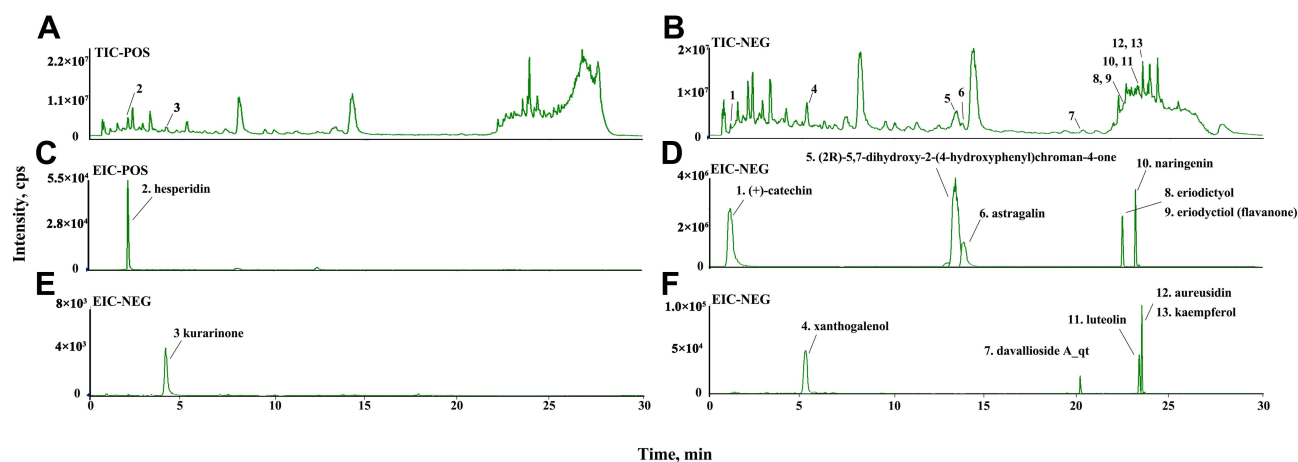


Figure 2 Identification of active compounds of TFRD with LC-MS. (A) Total ion chromatography on positive; (B) Total ion chromatography on negative; (C) Identification of hesperidin; (D) Identification of (+)-catechin, (2R)-5,7-dihydroxy-2-(4-hydroxyphenyl)chroman-4-one, astragalol, naringenin, eriodictyol and eriodictyol (flavanone); (E) Identification of kurarinone; (F) Identification of xanthogalenol, davallioside A_{qt}, luteolin, aureusidin and kaempferol.

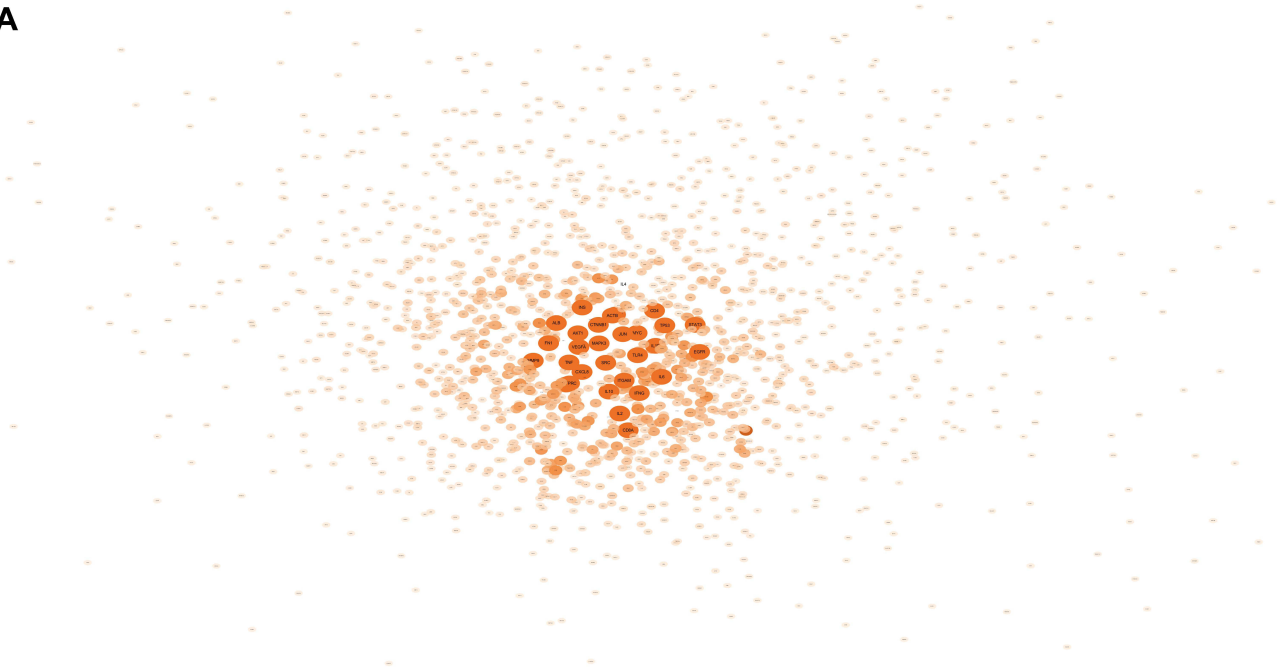
RA. The compound-target network was established with the active compounds of TFRD and intersection genes of RA and TFRD (Figure 4A).

Intersection genes of RA and TFRD were utilized to construct the PPI network. The PPI network consisted of 137 genes and 5596 connections, among which IL-6 is the most crucial target, and has 108 connections with other targets (Figure 4B). Due to sensitiveness of IL-6 to inflammatory response, IL-6 was selected as the indicator of subsequent experiments. The top 30 targets in the network included targets involving inflammatory mediators in the development of RA (IL6, TNF, IL10, PTGS2, IL1B, CCL2), inflammatory signaling pathways (AKT1, MAPK3, STAT3, MAPK1, MAPK8, MAPK14), cell apoptosis (TP53, CASP3, CCND1, FOS, BCL2L1), synovial neovascularization (VEGFA), cell autophagy (MTOR) and transcription regulation (RELA). The barplot of the top 30 targets is shown in Figure 4C.

Table 3 Chemical Identification of Total Flavonoids of Rhizoma Drynariae

No	RT (Min)	Name	Formula	Ion	Cal. m/z	Mea. m/z	Error (ppm)	MS/MS
1	2.05	(+)-catechin	C ₁₅ H ₁₄ O ₆	M-H	289.0717	289.072	4.62	289.072, 139.0388
2	2.08	Hesperidin	C ₂₈ H ₃₄ O ₁₅	M+H	611.197	611.197	0.07	611.197, 301.0499
3	4.1	Kurarinone	C ₂₆ H ₃₀ O ₆	M+H	439.2115	439.212	1.104	439.212
4	5.29	Xanthogalenol	C ₂₁ H ₂₂ O ₅	M-H	353.1394	353.1391	-2.123	353.1391
5	13.38	(2R)-5,7-dihydroxy-2-(4-hydroxyphenyl)chroman-4-one	C ₁₅ H ₁₂ O ₅	M-H	271.0611	271.0616	1.500	271.0616, 151.0033
6	13.69	Astragalol	C ₂₁ H ₂₀ O ₁₁	M-H	447.0932	447.093	1.757	447.093, 284.0831, 255.0303
7	20.27	Davallioside A _{qt}	C ₁₉ H ₁₉ NO ₇	M-H	372.1088	372.1086	3.285	534.1622, 354.1033
8	22.58	Eriodictyol	C ₁₅ H ₁₂ O ₆	M-H	287.0561	287.056	3.433	287.056, 151.0036, 135.0450
9	22.59	Eriodictyol (flavanone)	C ₁₅ H ₁₂ O ₆	M-H	287.0561	287.0566	3.974	287.0566, 151.0036
10	23.48	Naringenin	C ₁₅ H ₁₂ O ₅	M-H	271.0611	271.0616	4.534	271.0616, 151.0038
11	23.55	Luteolin	C ₁₅ H ₁₀ O ₆	M-H	285.0404	285.0411	4.383	285.0411, 151.0035
12	23.66	Aureusidin	C ₁₅ H ₁₀ O ₆	M-H	285.0404	285.04	2.23	285.0404, 151.0031
13	23.67	Kaempferol	C ₁₅ H ₁₀ O ₆	M-H	285.0404	285.0409	2.747	285.0409, 151.0042

A



B

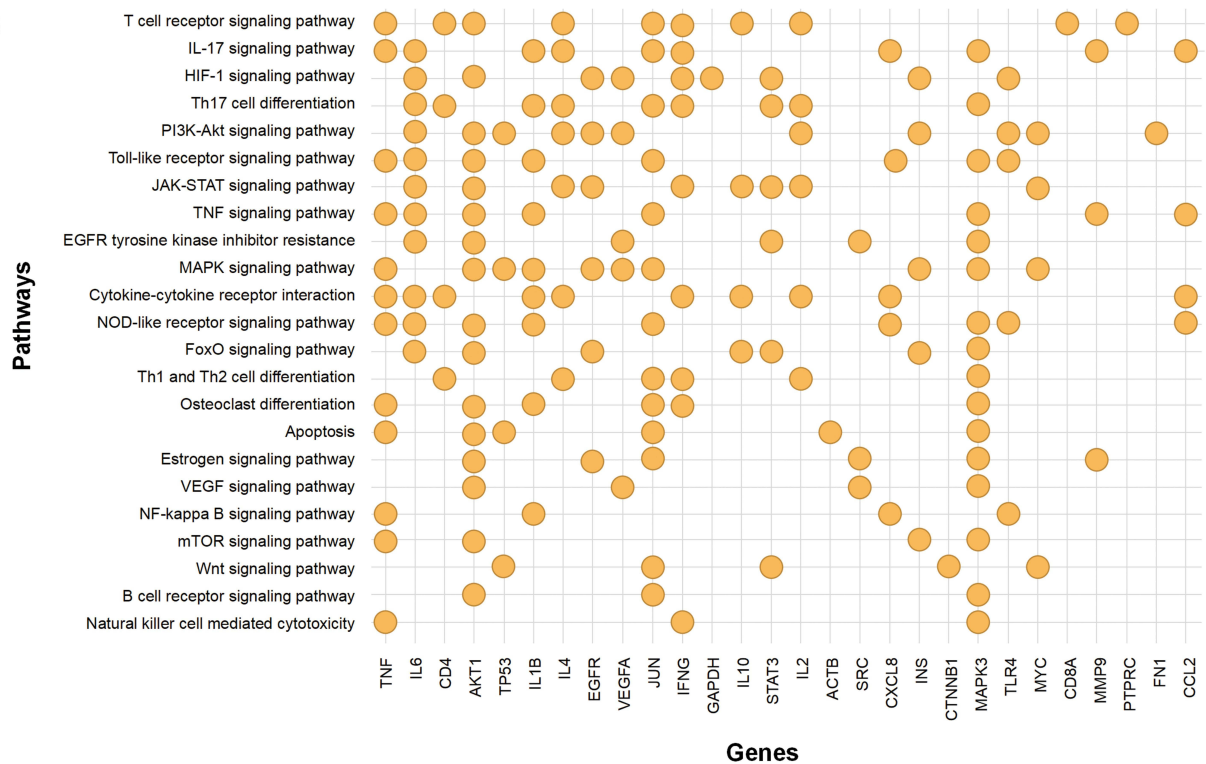


Figure 3 (A) PPI network of genes closely related to RA. **(B)** 30 genes of maximum connections of PPI network and RA-related pathways predicted by KEGG enrichment analysis.

KEGG Enrichment Analysis

The 154 intersection genes of RA and TFRD were used for KEGG enrichment analysis and then the top 30 pathways identified (Figure 5A). Among the top 30 pathways, IL-17 signaling pathway, PI3K-AKT signaling, TNF signaling pathway, T cell receptor signaling pathway, Th17 cell differentiation, MAPK signaling pathway and HIF-1 signaling

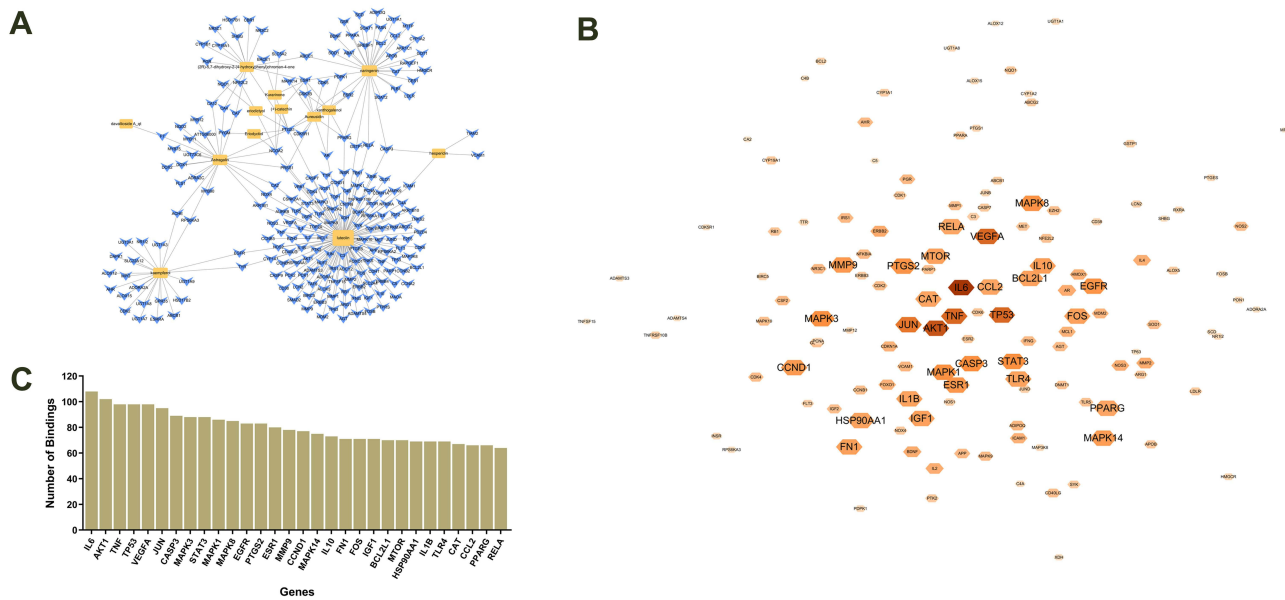


Figure 4 (A) Compound-target network of TFRD for treatment of RA. (B) PPI network of intersection genes of RA and TFRD. (C) Barplot of the top 30 targets of the maximum number of bindings in the PPI network.

pathway were included in the key pathways of RA predicted above. Then, the pathways and their corresponding gene targets were used to construct a network (Figure 5B).

Screening of Key Compounds

In order to predict key compounds of TFRD for treatment of RA, Optimization Space was built on the basis of the C-T network and genes in the PPI network of RA (Figure 6A). Subsequently, the weight of each compound was calculated in accordance with the number of targets connecting with each compound in the C-T network and connection combined

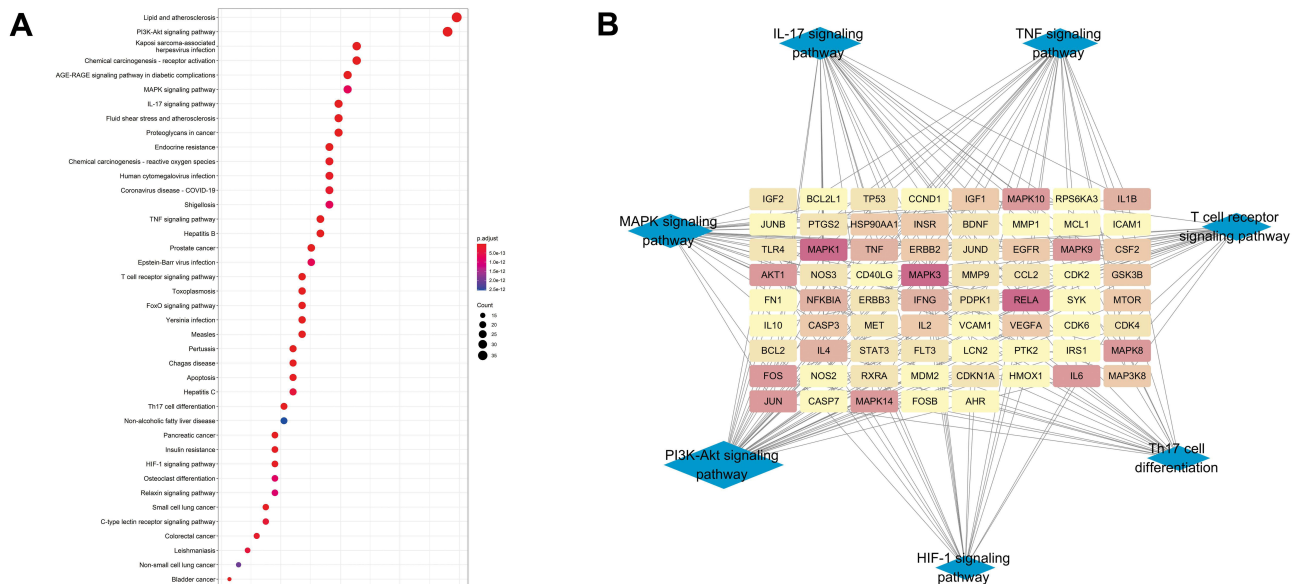


Figure 5 (A) Bubble diagram for the top 30 KEGG pathways of intersection genes of RA and TFRD. (B) Network of 7 RA-related pathways identified from KEGG enrichment analysis and their corresponding targets.

score of each gene in the PPI network, whose results showed luteolin (TFRD8) contributed to 67.18 % target weight, and thus was referred as the key compound of TFRD in treating RA (Figure 6B).

At the same time, 13 compounds involving the C-T network and key targets predicted by KEGG in the regulatory network were subjected to molecular docking. The results indicated hesperidin (TFRD11) had high binding energy with key proteins, suggesting that hesperidin was the other key compound in the regulatory network of TFRD for treatment of RA (Figure 6C).

Inflammatory Response, Joints Swelling and Pathological Changes of Ankles

In vivo experimental results indicated that the level of CRP in the serum of CIA rats remarkably increased compared with normal rats; however, after intervention with TFRD, the level of CRP decreased, but the therapeutic effect of TFRD group was inferior to that of MTX group (Figure 7A). The score of joint swelling of rats significantly increased after rats were established in the CIA model. TFRD and MTX can markedly inhibit the joint swelling to the same extent (Figure 7B). The results of pathology of ankles showed CIA rats exhibited synovial hyperplasia, bone erosions, and disruption of synovial lining compared with control rats (Figure 7C). TFRD-treated group can reverse these adverse changes to some extent; however, the effects of MTX were superior to those of TFRD.

The Proportion of Th17 Cells and the Expression of IL-17A and TNF- α in Lymphocytes

The results of flow cytometry suggested that the proportion of Th17 cells in lymphocytes from CIA rats exhibited a significant increase compared with the normal rats. The intervention of TFRD and MTX can decrease the proportion of Th17 cells (Figure 8A and B).

After peripheral blood lymphocytes (PBLs) from rats were separated, lymphocytes were stimulated with *PMA/ionomycin* for 6h and IL-17A and TNF- α contents in the supernatants were detected. The results showed that the contents of IL-17A and TNF- α secreted by lymphocytes in CIA group were significantly higher than in the normal group and the abnormal increases were reversed by TFRD and MTX to some extent (Figure 8C and D). The results suggested that TFRD inhibits IL-17A and TNF- α secreted by lymphocytes in blood of CIA rats, while MTX showed a better curative effect than TFRD in terms of inhibiting the secretion of IL-17A and TNF- α .

Cell Authentication

The results of immunofluorescence demonstrated that all cells were strongly positive for vimentin, suggesting that the cells had fibrogenic properties. The flow cytometry results showed that the most cells were positive for vimentin, CD68 and CD90. The cells showing positive for vimentin, CD68 and CD90 were determined as $(98.67 \pm 0.12\%, n = 3)$, $(99.53 \pm 0.03\%, n = 3)$ and $(95.57 \pm 0.18\%, n = 3)$ respectively. Moreover, $(95.23 \pm 0.09\%, n = 3)$ of the cells showed positive for vimentin (+), CD68(+) and CD90(+). Meanwhile, SW982 cells which were set as negative control presented vimentin (-), CD68(-) and CD90(+) mostly (Figure 9). The results of cell authentication indicated the cells were qualified for subsequent experiments.

Cell Proliferation Experiment

The results of MTS showed that low-dose TFRD promoted the proliferation of fibroblast-like synoviocytes, which is consistent with the previous results obtained in other cells. It is speculated that this may be related to TFRD promoting the energy metabolism of cells. The maximum concentration of TFRD for intervening in fibroblast-like synoviocytes was 500 $\mu\text{g/mL}$ (Figure 10A). Therefore, 500 $\mu\text{g/mL}$ is selected as the high-dose intervention concentration, 250 $\mu\text{g/mL}$ and 125 $\mu\text{g/mL}$ as the medium-dose and low-dose intervention concentration of the intervention fibroblast-like synoviocytes. The addition of 10 ng/mL IL-17A or TNF- α also promoted the proliferation of the fibroblast-like synoviocytes to a certain extent (Figure 10B).

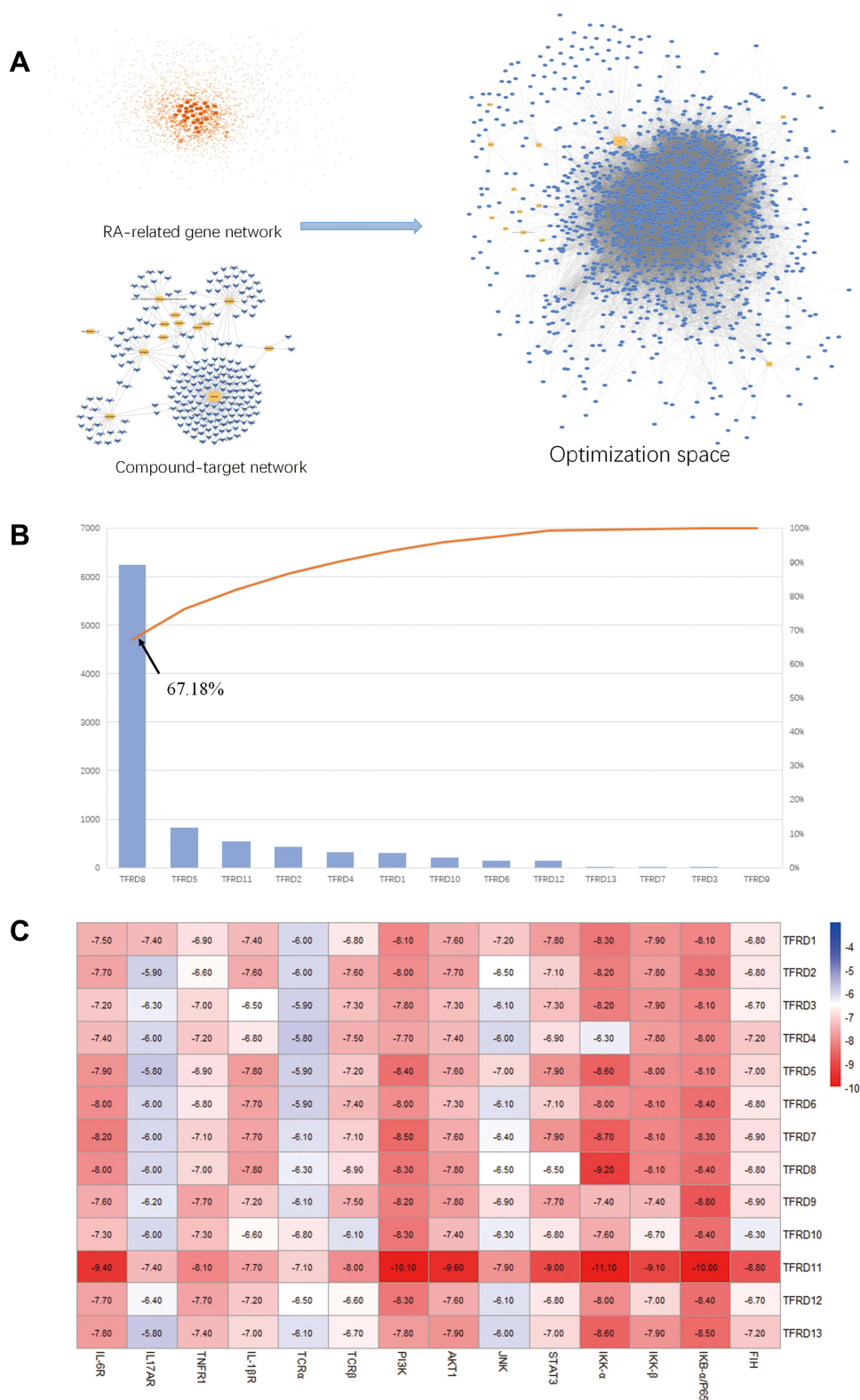


Figure 6 (A) Regulatory network of Optimization space based on RA-related gene network and compound-target network. (B) The contribution accumulation results of the active compounds in the network of Optimization space. (C) Heat map of binding energy between targets and compounds.

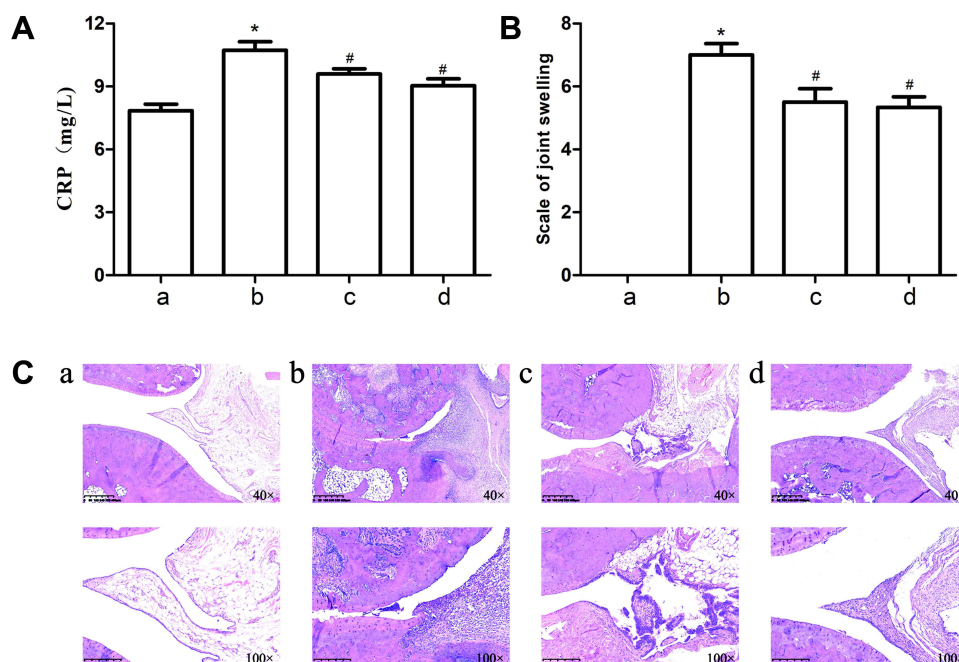


Figure 7 (A) CRP contents in the serum of rats in each group. (B) the score of joint swelling of rats in each group. (C) HE staining of synovium of ankles of rats in each group. a: Normal group, b: CIA model group, c: TFRD-treated group, d: MTX-treated group (* $P < 0.05$: increase compared with the control group; # $P < 0.05$: decrease compared with the control group).

Effects of TFRD on Fibroblast-Like Synoviocytes Stimulated with $TNF-\alpha$ and IL-17A

After fibroblast-like synoviocytes were stimulated with 10 ng/mL IL-17A or 10 ng/mL $TNF-\alpha$, mRNA and protein expression levels of IL-6 in cell culture supernatant markedly rose. As a positive control, DEX exhibited a remarkable inhibitory effect on the expression of IL-6. TFRD can inhibit the expression of IL-6 in a dose-dependent effect, however, the suppressive effect of TFRD was inferior to that of DEX (Figure 11).

Effects of TFRD on PI3K/AKT and MAPK Signaling Pathways in Fibroblast-Like Synoviocytes

The fibroblast-like synoviocytes were pretreated with TFRD or DEX and then stimulated with 10 ng/mL IL-17A or $TNF-\alpha$. The contents of PI3K, p-PI3K, AKT, p-AKT (Ser473), p38 MAPK, p-p38 MAPK were detected by WB method, whose results showed that stimulation with 10 ng/mL IL-17A and $TNF-\alpha$ did not change the expression of PI3K, AKT, p38 MAPK proteins, whereas the expression of p-PI3K, p-AKT (Ser473), p-p38 MAPK remarkably increased, suggesting the abnormal activation of PI3K/AKT and MAPK signaling pathways. DEX, the positive control drug, had an inhibitory effect on the expression of p-PI3K (Try458), p-AKT (Ser473) and p-p38 MAPK. The pretreatment with 125 μ g/mL TFRD can also decrease the expression of p-PI3K (Try458), p-AKT (Ser473), p-p38 MAPK (Figure 12), which indicated that TFRD can inhibit the abnormal activation of PI3K/AKT and MAPK signaling pathways mediated by IL-17A and $TNF-\alpha$.

Effects of TFRD on NF- κ B Signaling Pathway

After fibroblast-like synoviocytes were pretreated with 125 μ g/mL of TFRD or 100 nmol/mL of DEX, the cells were stimulated with 10 ng/mL IL-17A or $TNF-\alpha$. Western blotting was used to detect I κ B- α in cytoplasm and NF- κ B p65 in nuclei, while the location of NF- κ B p65 in the cells was determined by immunofluorescence.

WB results showed that 10 ng/mL of IL-17A or $TNF-\alpha$ decreased I κ B- α in cytoplasm but increased NF- κ B p65 in nuclei. Both 125 μ g/mL of TFRD and 100 nmol/mL of DEX can reverse these changes (Figure 13). Immunofluorescence showed that untreated fibroblast-like synoviocytes displayed the uniform distribution of NF- κ B p65 within cells, but

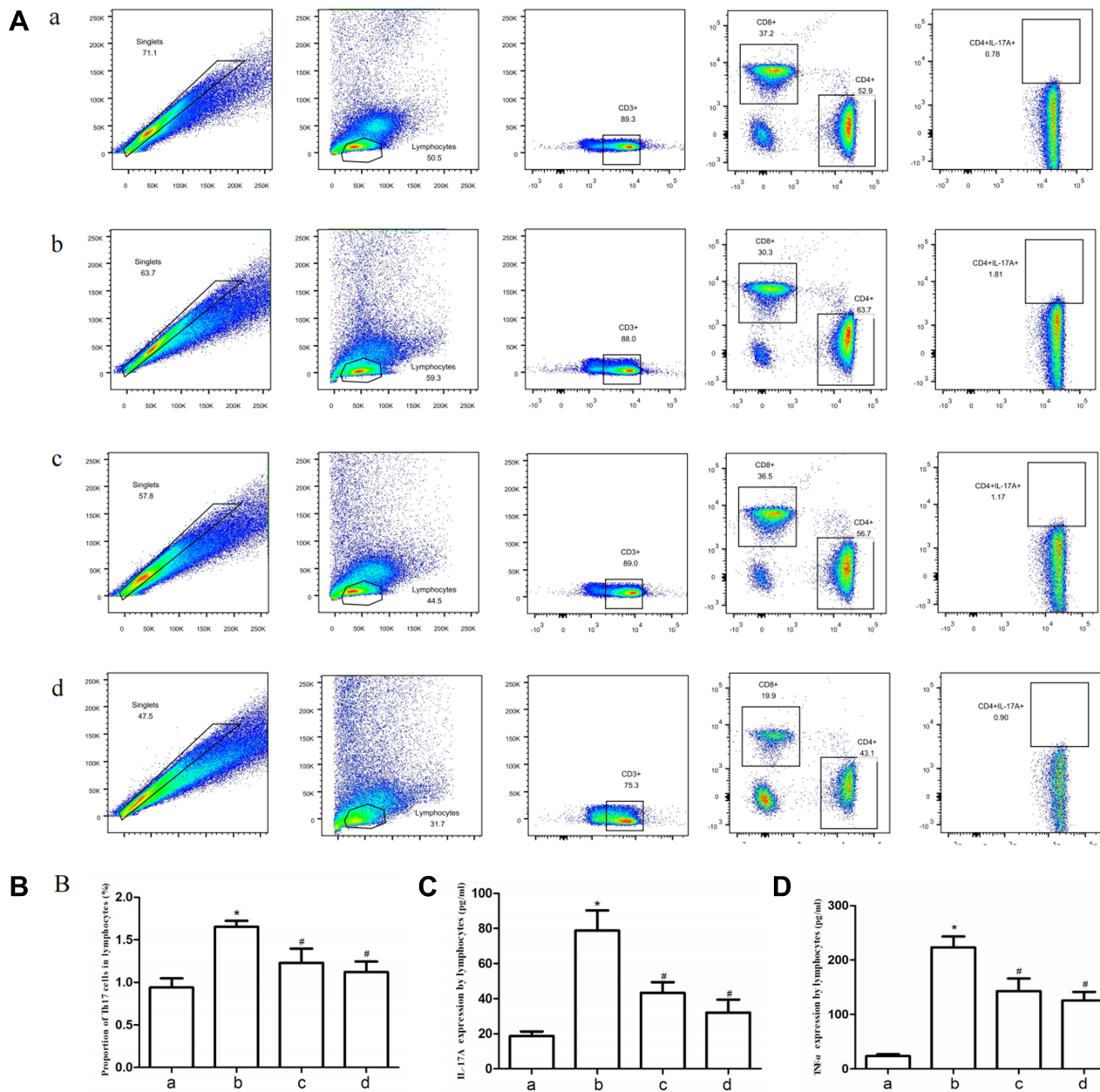


Figure 8 (A) Th17 cells in lymphocytes measured by flow cytometry. **(B)** The proportion of Th17 positive cells. **(C and D)** Peripheral blood lymphocytes were separated from rats and stimulated with PMA/ionomycin for 6 h; the contents of IL-17A and TNF- α in the supernatant were measured by ELISA. a: Normal group, b: CIA model group, c: TFRD-treated group, d: MTX-treated group (*P < 0.05: increase compared with the control group; #P < 0.05: decrease compared with the control group).

10 ng/mL of IL-17A and TNF- α had NF- κ B p65 resettled into nuclei of fibroblast-like synoviocytes and TFRD prevented nuclear translocation of the NF- κ B p65 part of fibroblast-like synoviocytes (Figure 14).

Effects of TFRD on HIF-1 α mRNA Expression

After fibroblast-like synoviocytes were pretreated with 125 μ g/mL of TFRD or 100 nmol/mL of DEX, the cells were stimulated with 10 ng/mL of IL-17A and TNF- α respectively. The mRNA expression levels of HIF-1 α were detected by qRT-PCR, whose results indicated that 10 ng/mL of IL-17A and TNF- α significantly increased HIF-1 α mRNA in fibroblast-like synoviocytes while 125 μ g/mL of TFRD and 100 nmol/mL of DEX reversed the change. DEX showed an effect superior to TFRD (Figure 15).

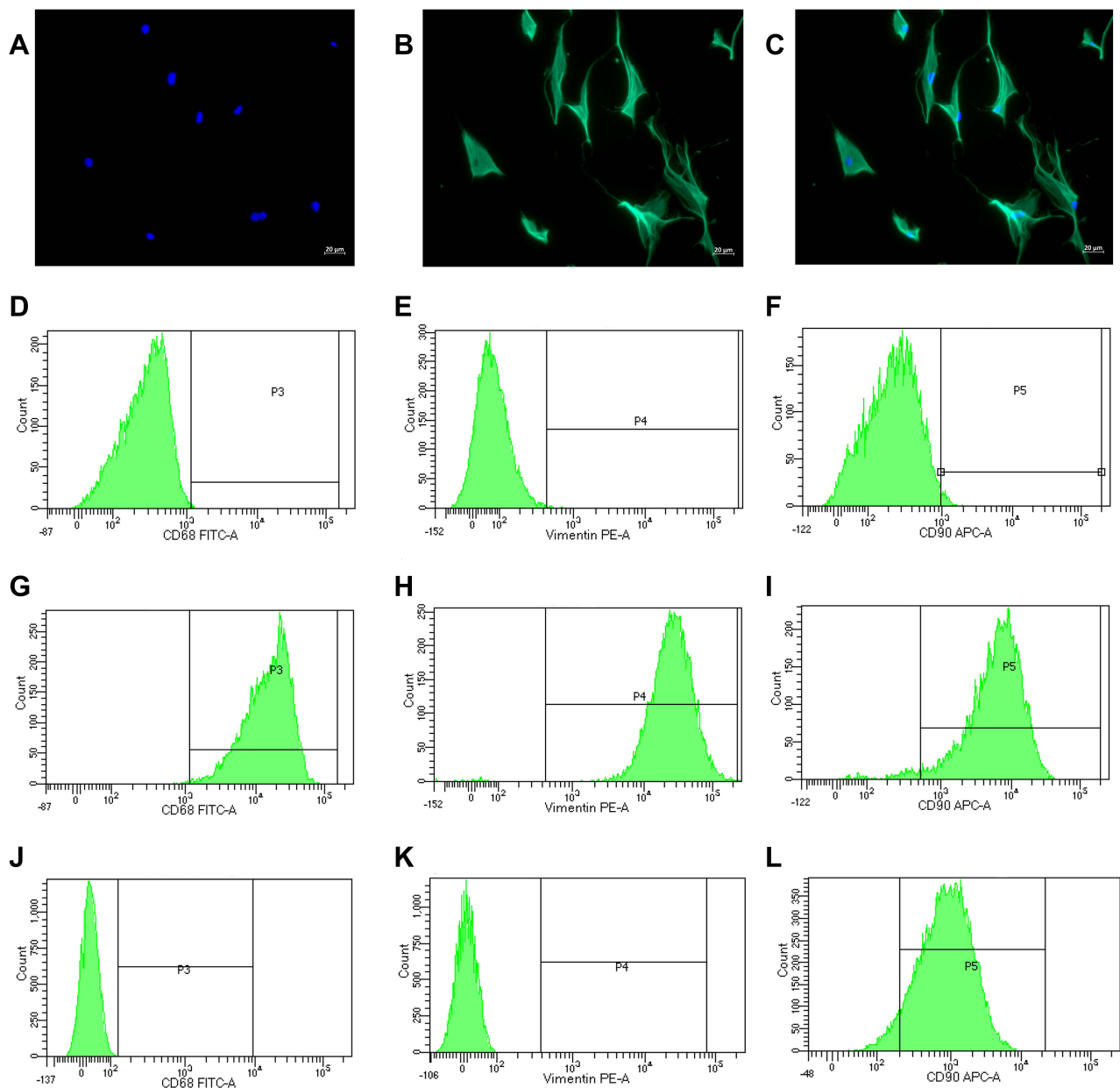


Figure 9 The localization of vimentin and DAPI was visualized under fluorescence microscopy after immunofluorescence staining. **(A)** DAPI staining of nuclei (blue). **(B)** Anti-vimentin antibody (green). **(C)** the merge of **(A)** and **(B)**. Superficial markers of RA-FLS cells were detected by flow cytometry, with SW982 cells being negative control. **(D)** RA-FLS without inclusion of CD68 antibody as isotype control. **(E)** RA-FLS without inclusion of vimentin antibody as isotype control. **(F)** RA-FLS without inclusion of CD90 antibody as isotype control. **(G)** RA-FLS showing positive for CD68 ($99.53 \pm 0.03\%$, $n = 3$). **(H)** RA-FLS showing positive for vimentin ($98.67 \pm 0.12\%$, $n = 3$). **(I)** RA-FLS showing positive for CD90 ($95.57 \pm 0.18\%$, $n = 3$). **(J)** SW982 showing negative for CD68. **(K)** SW982 showing negative for vimentin. **(L)** most SW982 showing positive for CD90.

Discussion

In this study, we predicted key targets and pathways in the treatment of RA with TFRD via network pharmacology. Experimental verification validated the predicted mechanism of the treatment of RA with TFRD in vivo and in vitro.

After TFRD intervention, the degree of joint swelling and CRP in the serum of rats reduced to a certain extent, and the pathological findings of synovitis were decreased, suggesting that TFRD can suppress the inflammatory response in the CIA model. In China, TFRD has been approved for the treatment of osteoporosis for nearly 20 years and its common adverse reactions only include dry mouth and constipation. As the first-line drug of RA, MTX has a series of side effects such as hepatic dysfunction, myelosuppression and gastrointestinal reactions; many patients discontinue their medication

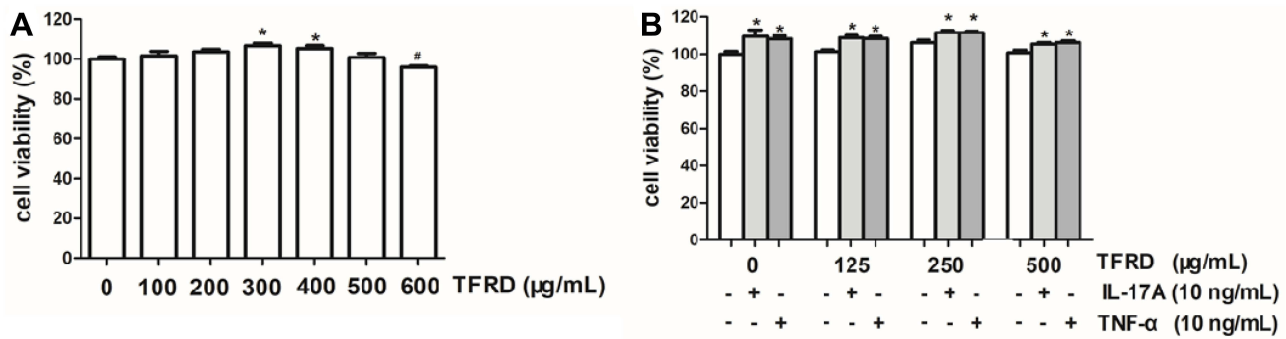


Figure 10 (A) Effects of different concentrations of TFRD on the cell proliferation of RA-FLSs. **(B)** 10 ng/mL of IL-17A or TNF-α on cell proliferation of RA-FLSs with/without TFRD (*P <0.05: increase compared with the control group; #P <0.05: decrease compared with the control group).

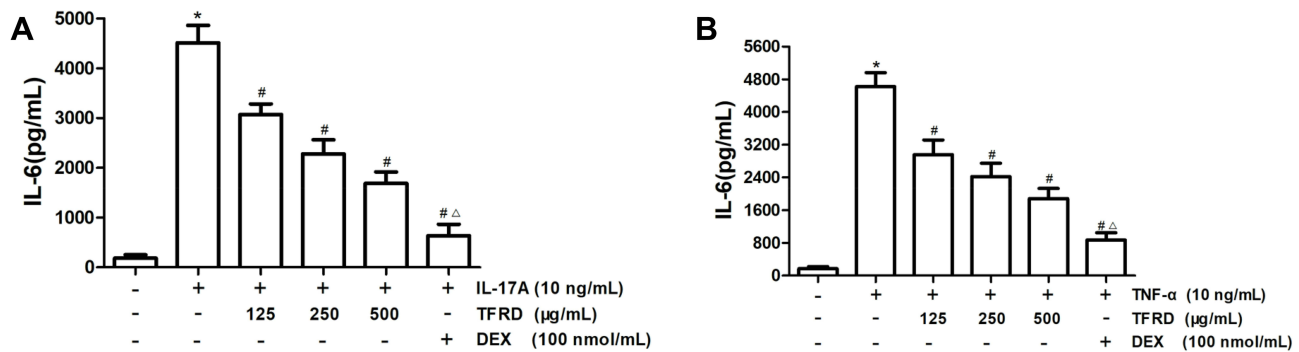


Figure 11 After 1 h of the pretreatment with 125, 250 and 500 µg/mL of TFRD or 100 nmol/mL of DEX, RA-FLSs were stimulated with 10 ng/mL of IL-17A or TNF-α for 12 h. **(A)** IL-6 level in the supernatant after the stimulation of 10 ng/mL of IL-17A. **(B)** IL-6 level in the supernatant after the stimulation of 10 ng/mL of TNF-α (*P <0.05: increase compared with the control group; #P <0.05: decrease compared with the TNF-α or IL-17 induced group; ΔP <0.05: decrease compared with the high concentration of TFRD group).

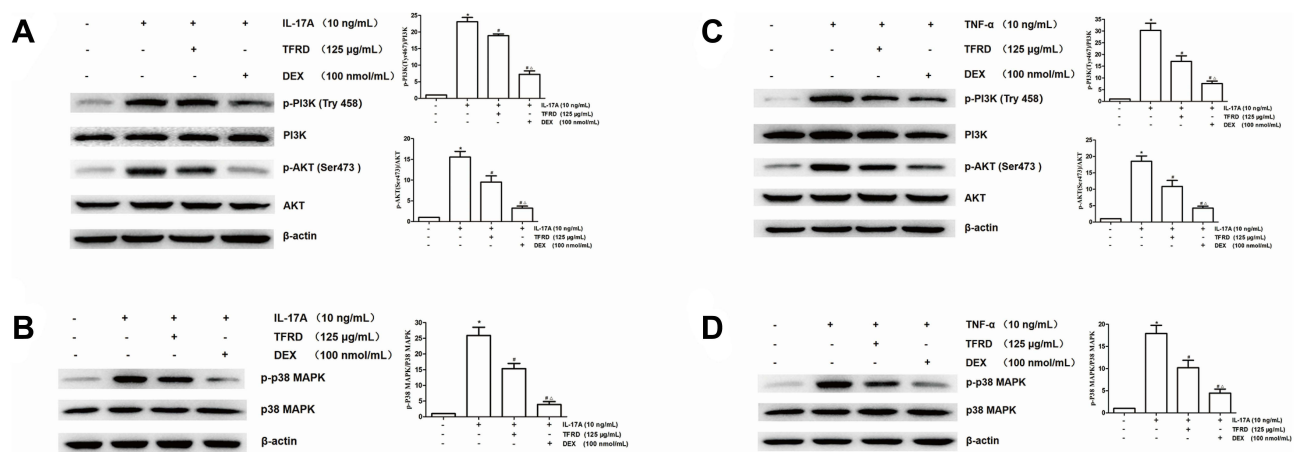


Figure 12 After 1 h of the pretreatment with 125 µg/mL of TFRD or 100 nmol/mL of DEX, RA-FLSs were stimulated with 10 ng/mL of IL-17A or TNF-α for 12 h. **(A)** The expression levels of PI3K/AKT pathway-related proteins and their phosphorylated proteins after the stimulation of 10 ng/mL of IL-17A. **(B)** The expression levels of MAPK pathway-related proteins and their phosphorylated proteins after the stimulation of 10 ng/mL of IL-17A. **(C)** The expression levels of PI3K/AKT pathway-related proteins and their phosphorylated proteins after the stimulation of 10 ng/mL of TNF-α. **(D)** The expression levels of MAPK pathway-related proteins and their phosphorylated proteins after the stimulation of 10 ng/mL of TNF-α (*P <0.05: increase compared with the control group; #P <0.05: decrease compared with the TNF-α or IL-17 induced group; ΔP <0.05: decrease compared with TFRD-treated group).

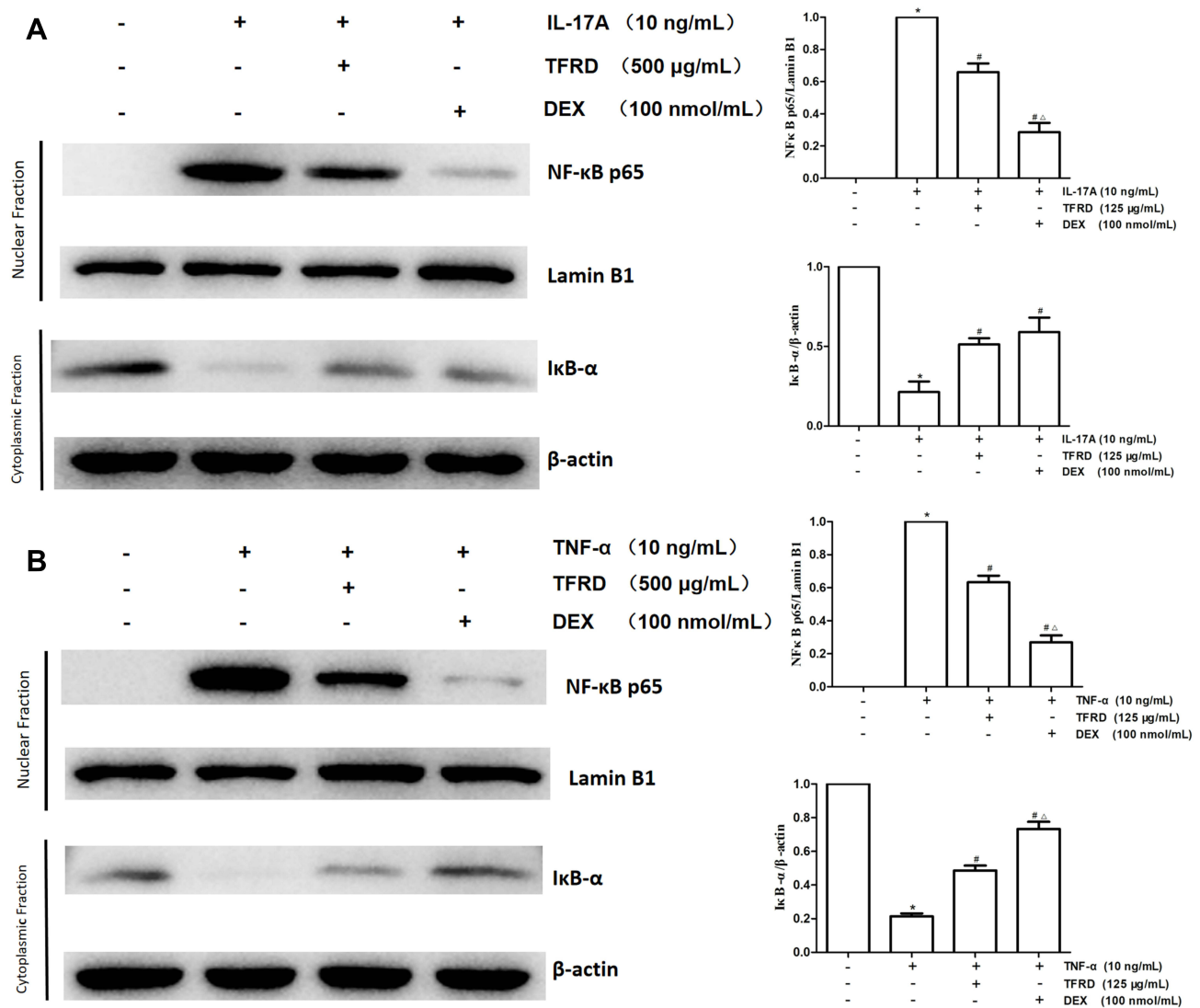


Figure 13 After 1 h of the pretreatment with 125 μg/mL of TFRD or 100 nmol/mL of DEX, RA-FLSs were stimulated with 10 ng/mL of IL-17A or TNF-α for 12 h. **(A)** The levels of NFκB p65 in nuclei and IκB-α in cytoplasm after the stimulation of 10 ng/mL of IL-17A. **(B)** The levels of NFκB p65 in nuclei and IκB-α in cytoplasm after the stimulation of 10 ng/mL of TNF-α (*P <0.05: increase compared with the control group; #P <0.05: decrease compared with the TNF-α or IL-17 induced group; ΔP <0.05: decrease compared with TFRD-treated group).

with MTX due to its side effects.^{36,37} Although our experiments revealed TFRD's efficacy was inferior to MTX, the few adverse effects indicate the potential clinical utility of TFRD in the treatment of RA.

T-cell-mediated adaptive immune response is crucial for the occurrence and development of RA, and Th cells play a significant role in stimulating B cells to produce autoantibodies.³⁸⁻⁴⁰ Simultaneously, T cells can also regulate the body's inflammatory response by secreting multiple cytokines. Previous studies have demonstrated abnormal differentiation of naive CD4⁺ T-cells in patients with RA, including the immune imbalance of Th1/Th2 cells and Th17/Treg cells.⁴¹

In the experiments *in vivo*, the increased proportion of Th17 cells in lymphocytes showed the abnormal differentiation of Th17 cells in CIA rats. TFRD can reverse the change, which suggested that TFRD may inhibit the Th17 cell differentiation through the T cell receptor signaling pathway. Our previous studies found that TNF-α and IL-17A were hardly available in the serum of CIA rats by ELISA assay; hence, lymphocytes were isolated from rat peripheral blood and then were stimulated by combined administration of PMA and Ionomycin. Then, the contents of IL-17 and TNF-α in cell culture supernatant were determined. The results suggested that the expression of IL-17A and TNF-α in the lymphocytes from CIA rats showed a marked increase, which indicated the increased number and/or enhanced activity

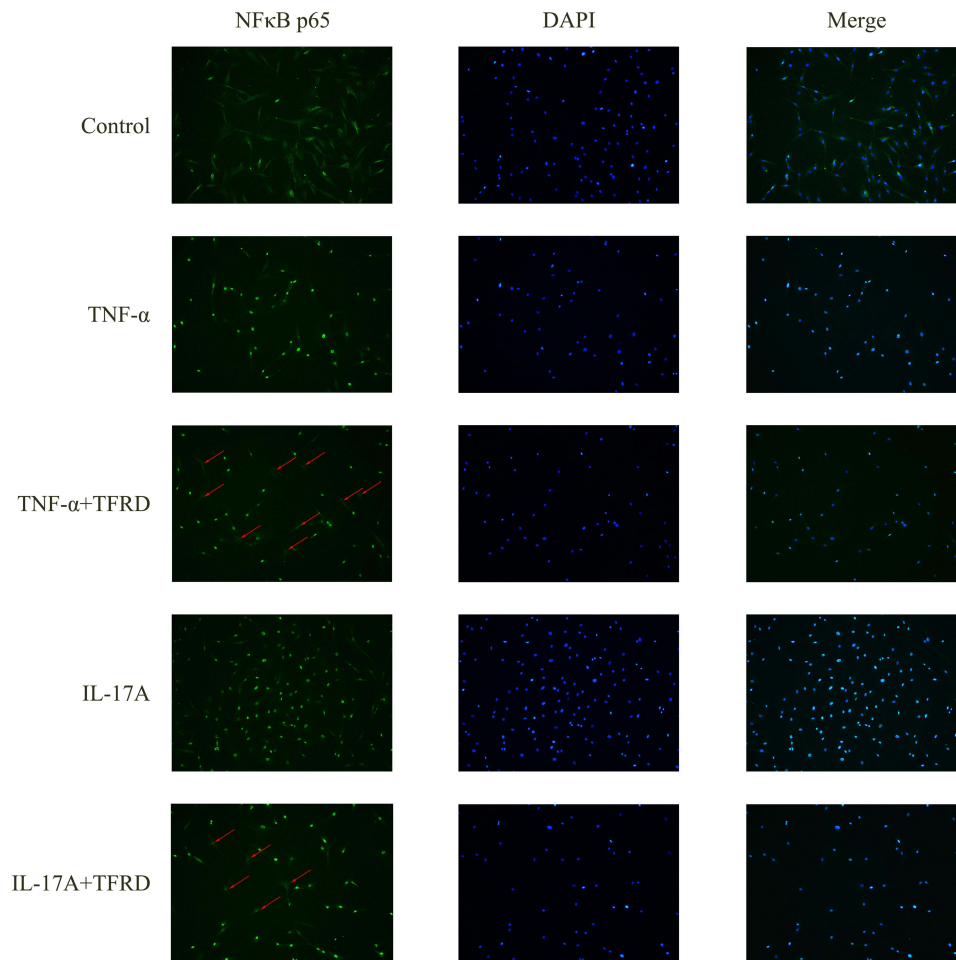


Figure 14 After 1 h of the pretreatment with 125 $\mu\text{g/mL}$ of TFRD, RA-FLSs were stimulated with 10 ng/mL of IL-17A or TNF- α for 30 min. The distribution of NF κ B p65 in cells was observed via immunofluorescence staining.

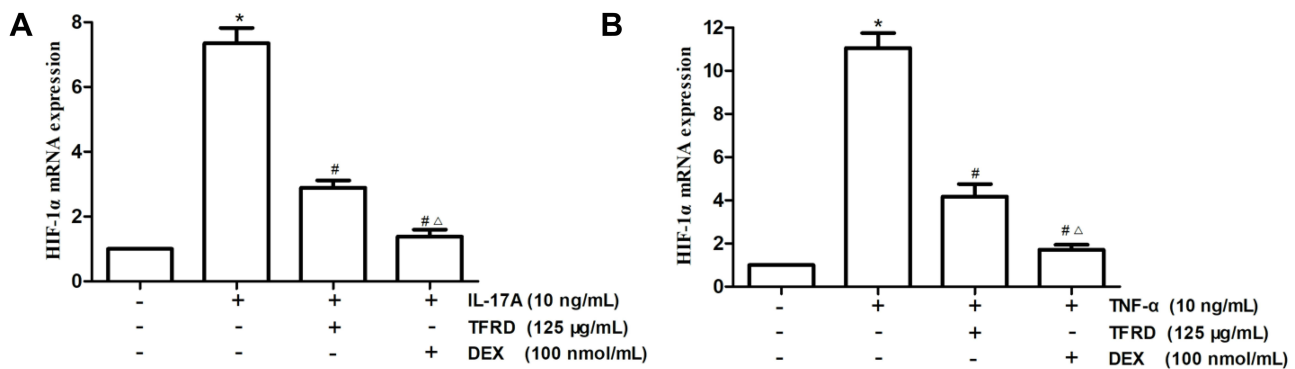


Figure 15 After 1 h of the pretreatment with 125 $\mu\text{g/mL}$ of TFRD or 100 nmol/mL of DEX, RA-FLSs were stimulated with 10 ng/mL of IL-17A or TNF- α for 12 h. **(A)** The levels of HIF-1 α mRNA after the stimulation of 10 ng/mL of IL-17A. **(B)** The levels of HIF-1 α mRNA after the stimulation of 10 ng/mL of TNF- α (* P < 0.05: increase compared with the control group; # P < 0.05: decrease compared with the TNF- α or IL-17 induced group; ΔP < 0.05: decrease compared with TFRD-treated group).

of Th17 cells and TNF- α -related lymphocytes. The lymphocytes of TFRD-treated and MTX-treated rats exhibited a significant decrease of IL-17A and TNF- α , indicating the decreased number and/or reduced activity of Th17 cells and TNF- α -related lymphocytes.

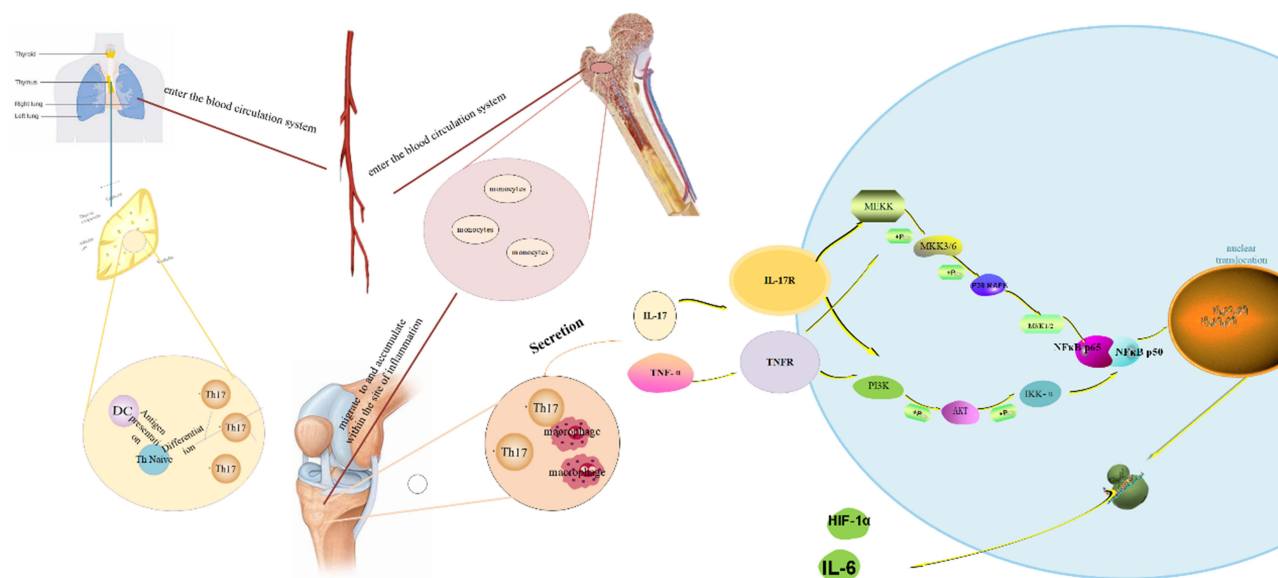


Figure 16 A schematic hypothesis about connections between relevant signaling pathways.

At the initial stage of the inflammatory response of RA, a variety of cells (macrophages, T lymphocytes, B lymphocytes and synovial cells) secrete a large amount of IL-6, which further stimulates the differentiation of B cells to produce relevant autoantibodies, and stimulates the proliferation and activation of T cells to enhance the autoimmune response, being one of the reasons for the aggravation of RA disease.⁴² Monoclonal antibody of IL-6 is recommended for the treatment of RA.⁴³ Randomized controlled trials showed that monoclonal antibody of IL-6 improved disease activity better than monoclonal antibody of TNF- α in the treatment of RA.^{44,45} A number of studies have shown that IL-6 is closely related to the degree of disease activity and prognosis of RA, which can be used as an indicator to evaluate clinical efficacy.^{46,47}

In our study, network pharmacology suggested that IL-6 is a core target in the treatment of RA with TFRD. Previous research revealed that IL-6 can reflect the degree of inflammation of FLSs *in vitro*, which can be influenced by drug intervention.⁴⁸ In *in vitro* experiments, pro-inflammatory factors were used to induce RA-FLSs to stimulate the inflammatory response of the synovium and IL-6 was selected as an indicator of the degree of inflammation. In our *in vitro* experiments, IL-17A and TNF- α were used to stimulate RA-FLSs to activate IL-17 and TNF signaling pathways, respectively. After stimulation by inflammatory factors, the expression of IL-6 was significantly elevated, while TFRD was able to inhibit IL-6 expression, showing a dose-dependent effect.

The MAPK and PI3K/AKT pathways in fibroblast synoviocytes can be activated by pro-inflammatory factors and subsequently activate the NF- κ B pathway.⁴⁹ The activation of the NF- κ B pathway can promote transcription and synthesis of multiple inflammation-related mediators, including IL-6 and HIF-1 α .⁵⁰ HIF-1 α can stimulate the transcription and synthesis of VEGF through the HIF signaling pathway, which is one of important mechanisms of synovial neovascularization.⁵⁰

For *in vivo* studies of botanical drug extracts, the consensus guidelines suggested that 100–200 μ g/mL should be assumed as being the upper limit for meaningful pharmacological studies.⁵¹ Therefore, TFRD at low concentration (125 μ g/mL) was used for subsequent experiments to probe for potential mechanisms underlying these observations. The results showed the abnormal activation of the MAPK, PI3K/AKT and NF κ B signaling pathways after stimulation of IL-17A and TNF- α , which was consistent with previous literatures. At the same time, the expression of HIF-1 α regulated by NF- κ B significantly increased. The intervention of TFRD can inhibit the abnormal activation of MAPK, PI3K/AKT and NF- κ B signaling pathways and the expression of HIF-1 α to a certain extent.

Conclusion

Taken together, we can conclude from our results that TFRD can inhibit the inflammatory response and pathological changes of RA rats, and its mechanism may be closely related to inhibiting the differentiation of Th17 cells and the secretion of inflammatory factors (TNF- α , IL-17A) by lymphocytes. Meanwhile, TFRD is able to inhibit the activation of MAPK, PI3K/AKT and NF- κ B signaling pathways and TNF- α and IL-17A-mediated secretion of IL-6 and HIF-1 α by fibroblast-like synoviocytes. The relationship between these key molecules and pathways is shown in Figure 16.

Funding

This study was supported by the National Natural Science Foundation of China (No. 81804042, 81673941), National Famous Traditional Chinese Medicine Experts inheritance studio of Xiaoping Yan (2019-PP-001), National Regional Chinese Medicine Diagnostic and Treatment Centre for Rheumatic Diseases Project (2019-ZX-006), National Key Clinical Specialty Capacity Building Project (2011-ZDZK-001).

Disclosure

The authors report no conflicts of interest in this work.

References

1. Scott DL, Wolfe F, Huizinga TW. Rheumatoid arthritis. *Lancet*. 2010;376:1094–1108. doi:10.1016/S0140-6736(10)60826-4
2. Viatte S, Barton A. Genetics of rheumatoid arthritis susceptibility, severity, and treatment response. *Semin Immunopathol*. 2017;39:395–408. doi:10.1007/s00281-017-0630-4
3. Mathew AJ, Ravindran V. Infections and arthritis. *Best Pract Res Clin Rheumatol*. 2014;28:935–959. doi:10.1016/j.berh.2015.04.009
4. Zeng P-L, Bengtsson C, Klareskog L, Alfredsson L. Working in cold environment and risk of developing rheumatoid arthritis: results from the Swedish EIRA case-control study. *RMD Open*. 2017;3:e000488. doi:10.1136/rmdopen-2017-000488
5. McInnes IB, Schett G. Pathogenetic insights from the treatment of rheumatoid arthritis. *Lancet*. 2017;389:2328–2337. doi:10.1016/S0140-6736(17)31472-1
6. Schett G, Gravallese E. Bone erosion in rheumatoid arthritis: mechanisms, diagnosis and treatment. *Nat Rev Rheumatol*. 2012;8:656–664. doi:10.1038/nrrheum.2012.153
7. Burmester GR, Pope JE. Novel treatment strategies in rheumatoid arthritis. *Lancet*. 2017;389:2338–2348. doi:10.1016/S0140-6736(17)31491-5
8. Bathon JM, McMahon DJ. Making rational treatment decisions in rheumatoid arthritis when methotrexate fails. *N Engl J Med*. 2013;369:384–385. doi:10.1056/NEJMe1306381
9. Singh JA, Cameron C, Noorbaloochi S, et al. Risk of serious infection in biological treatment of patients with rheumatoid arthritis: a systematic review and meta-analysis. *Lancet*. 2015;386:258–265. doi:10.1016/S0140-6736(14)61704-9
10. Rubbert-Roth A, Xavier RM. Trial of upadacitinib or abatacept in rheumatoid arthritis. *N Engl J Med*. 2021;384(1):83. doi:10.1056/NEJMc2033206
11. Scott DL, Stevenson MD. Treating active rheumatoid arthritis with Janus kinase inhibitors. *Lancet*. 2017;390:431–432. doi:10.1016/S0140-6736(17)31659-8
12. Daily JW, Zhang T, Cao S-H, Park S. Efficacy and safety of GuiZhi-ShaoYao-ZhiMu decoction for treating rheumatoid arthritis: a systematic review and meta-analysis of randomized clinical trials. *J Altern Complement Med*. 2017;23:756–770. doi:10.1089/acm.2017.0098
13. Wang W, Wang X, Tang X, Jiang Q, Fan Y. Classifying rheumatoid arthritis by Traditional Chinese Medicine Zheng: a multi-center cross-sectional study. *J Tradit Chin Med*. 2019;39:425–432.
14. Zheng W, Mei Y, Chen C, Cai L, Chen H. The effectiveness and safety of Tripterygium wilfordii glycosides combined with disease-modifying anti-rheumatic drugs in the treatment of rheumatoid arthritis: a systematic review and meta-analysis of 40 randomized controlled trials. *Phytother Res*. 2021;35:2902–2924. doi:10.1002/ptr.6996
15. Liu B, Meng X, Ma Y-F, Li H-Z, Lu C. Clinical safety of total glucosides of paeony adjuvant therapy for rheumatoid arthritis treatment: a systematic review and meta-analysis. *BMC Complement Med Ther*. 2021;21:102. doi:10.1186/s12906-021-03252-y
16. Chen X, Li D, Zhang H, Duan Y-W, Huang Y. Co-amorphous systems of sinomenine with nonsteroidal anti-inflammatory drugs: a strategy for solubility improvement, sustained release, and drug combination therapy against rheumatoid arthritis. *Int J Pharm*. 2021;606:120894. doi:10.1016/j.ijpharm.2021.120894
17. Raterman HG, Bultink IE, Lems WF. Osteoporosis in patients with rheumatoid arthritis: an update in epidemiology, pathogenesis, and fracture prevention. *Expert Opin Pharmacother*. 2020;21:1725–1737. doi:10.1080/14656566.2020.1787381
18. Zhao YD, Xu WD. Clinical observation on qiangqu capsule combined with sulfasalazine on bone metabolism in patients with rheumatoid arthritis complicated with osteoporosis. *World J Trad Chin Med*. 2019;14:438–441.
19. Ru JL, Li P, Wang J, et al. TCMSp: a database of systems pharmacology for drug discovery from herbal medicines. *J Cheminform*. 2014;6:13. doi:10.1186/1758-2946-6-13
20. Xue R-C, Fang Z, Zhang MX, Yi ZH, Wen C-P, Shi T-L. TCMID: traditional Chinese medicine integrative database for herb molecular mechanism analysis. *Nucleic Acids Res*. 2013;41:D1089–95. doi:10.1093/nar/gks1100
21. Gan D, Xu X, Chen D, Feng P, Xu Z. Network pharmacology-based pharmacological mechanism of the Chinese medicine rhizoma drynariae against osteoporosis. *Med Sci Monit*. 2019;25:5700–5716. doi:10.12659/MSM.915170

22. Huang YF, Bai C, He F, Xie Y, Zhou H. Review on the potential action mechanisms of Chinese medicines in treating Coronavirus Disease 2019 (COVID-19). *Pharmacol Res.* 2020;158:104939. doi:10.1016/j.phrs.2020.104939
23. Chen GY, Chen JQ, Liu XY, Xu Y, Tao QW. Total flavonoids of rhizoma drynariae restore the MMP/TIMP balance in models of osteoarthritis by inhibiting the activation of the NF- κ B and PI3K/AKT pathways. *Evid Based Complement Alternat Med.* 2021;2021:6634837. doi:10.1155/2021/6634837
24. Zhang S, Lu Y, Chen W, et al. Network pharmacology and experimental evidence: PI3K/AKT signaling pathway is involved in the antidepressive roles of Chaihu Shugan San. *Drug Des Devel Ther.* 2021;15:3425–3441. doi:10.2147/DDDT.S315060
25. Thieme S, Walther D, Kuijjer M. Biclique extension as an effective approach to identify missing links in metabolic compound–protein interaction networks. *Bioinform Adv.* 2022;2(1):vbac001. doi:10.1093/bioadv/vbac001
26. Zhang YY, Ma JX, Zhu YT, et al. Investigation of the mechanisms and experimental verification of Cuscuta-Salvia in the treatment of polycystic ovary syndrome (PCOS) via network pharmacology. *J Ovarian Res.* 2022;15(1):40. doi:10.1186/s13048-022-00964-8
27. Shaleen J, Das A. Virtual screening of natural compounds as combinatorial agents from Indian medicinal plants against estrogen positive breast cancer. *Int J Integr Educ.* 2020;3(10):266–275. doi:10.31149/ijie.v3i10.750
28. Gao Y, Wang KX, Wang P, et al. A novel network pharmacology strategy to decode mechanism of Lang Chuang Wan in treating systemic lupus erythematosus. *Front Pharmacol.* 2020;11:512877. doi:10.3389/fphar.2020.512877
29. Xu A, Wen ZH, Su SX, et al. Elucidating the synergistic effect of multiple Chinese herbal prescriptions in the treatment of post-stroke neurological damage. *Front Pharmacol.* 2022;13:784242. doi:10.3389/fphar.2022.784242
30. Wu J, Wang K, Liu Q, et al. An integrative pharmacology model for decoding the underlying therapeutic mechanisms of Ermiao powder for rheumatoid arthritis. *Front Pharmacol.* 2022;13:801350. doi:10.3389/fphar.2022.801350
31. Krenn V, Morawietz L, Häupl T, Neidel J, Petersen I, König A. Grading of chronic synovitis—a histopathological grading system for molecular and diagnostic pathology. *Pathol Res Pract.* 2002;198(5):317–325. doi:10.1078/0344-0338-5710261
32. Ahmed YM, Messiha BA, Abo-Saif AA. Protective effects of simvastatin and hesperidin against complete Freund’s adjuvant-induced rheumatoid arthritis in rats. *Pharmacology.* 2015;96:217–225. doi:10.1159/000439538
33. Ahmad S, Alam K, Hossain MM, Fatima M, Nafees KA. Anti-arthritis and cardioprotective action of hesperidin and daidzein in collagen-induced rheumatoid arthritis. *Mol Cell Biochem.* 2016;423:115–127. doi:10.1007/s11010-016-2830-y
34. Tang KT, Lin CC, Lin SC, Wang JH, Tsai SW. Kurarinone attenuates collagen-induced arthritis in mice by inhibiting Th1/Th17 cell responses and oxidative stress. *Int J Mol Sci.* 2021;22:4002. doi:10.3390/ijms22084002
35. Jia Q, Wang T, Wang X, et al. Astragalosin suppresses inflammatory responses and bone destruction in mice with collagen-induced arthritis and in human fibroblast-like synoviocytes. *Front Pharmacol.* 2019;10:94. doi:10.3389/fphar.2019.00094
36. Sandoval DM, Alarcón GS, Morgan SL. Adverse events in methotrexate-treated rheumatoid arthritis patients. *Br J Rheumatol.* 1995;34:49–56. doi:10.1093/rheumatology/XXXIV.suppl_2.49
37. Nakarmi S, Pudasaini K, Adhikari B, Vaidya B. Adverse events profile of low-dose methotrexate in Nepalese patients with rheumatoid arthritis: an observational study. *J Nepal Health Res Counc.* 2020;18:360–365. doi:10.33314/jnhrc.v18i3.2743
38. Wehr P, Purvis H, Law SC, Thomas R. Dendritic cells, T cells and their interaction in rheumatoid arthritis. *Clin Exp Immunol.* 2019;196:12–27. doi:10.1111/cei.13256
39. Kondo Y, Yokosawa M, Kaneko S, et al. Review: transcriptional regulation of CD4+ T cell differentiation in experimentally induced arthritis and rheumatoid arthritis. *Arthritis Rheumatol.* 2018;70:653–661. doi:10.1002/art.40398
40. Weyand CM, Zeisbrich M, Goronzy JJ. Metabolic signatures of T-cells and macrophages in rheumatoid arthritis. *Curr Opin Immunol.* 2017;46:112–120. doi:10.1016/j.coi.2017.04.010
41. Weyand CM, Goronzy JJ. Immunometabolism in early and late stages of rheumatoid arthritis. *Nat Rev Rheumatol.* 2017;13:291–301. doi:10.1038/nrrheum.2017.49
42. Pandolfi F, Franza L, Carusi V, Altamura S, Andriollo G, Nucera E. Interleukin-6 in Rheumatoid Arthritis. *Int J Mol Sci.* 2020;21:5238. doi:10.3390/ijms21155238
43. Kerschbaumer A, Sepriano A, Smolen JS, et al. Efficacy of pharmacological treatment in rheumatoid arthritis: a systematic literature research informing the 2019 update of the EULAR recommendations for management of rheumatoid arthritis. *Ann Rheum Dis.* 2019;79:744–759. doi:10.1136/annrheumdis-2019-216656
44. Aletaha D, Bingham CO, Tanaka Y, et al. Efficacy and safety of sirukumab in patients with active rheumatoid arthritis refractory to anti-TNF therapy (SIRROUND-T): a randomised, double-blind, placebo-controlled, parallel-group, multinational, Phase 3 study. *Lancet.* 2017;389:1206–1217. doi:10.1016/S0140-6736(17)30401-4
45. Thorne C, Takeuchi T, Karpouzas GA, et al. Investigating sirukumab for rheumatoid arthritis: 2-year results from the Phase III SIRROUND-D study. *RMD Open.* 2018;4(2):e000731. doi:10.1136/rmdopen-2018-000731
46. Boyapati A, Schwartzman S, Msihid J, et al. Association of high serum interleukin-6 levels with severe progression of rheumatoid arthritis and increased treatment response differentiating sarilumab from adalimumab or methotrexate in a post hoc analysis. *Arthritis Rheumatol.* 2020;72:1456–1466. doi:10.1002/art.41299
47. Rajaei E, Mowla K, Hayati Q, et al. Evaluating the relationship between serum level of interleukin-6 and rheumatoid arthritis severity and disease activity. *Curr Rheumatol Rev.* 2020;16:249–255. doi:10.2174/1573397115666190206144223
48. Hattori T, Ogura N, Akutsu M, et al. Gene expression profiling of IL-17A-treated synovial fibroblasts from the human temporomandibular joint. *Mediators Inflamm.* 2015;2015:1–12. doi:10.1155/2015/436067
49. Fiechter RH, Jong HMD, Mens LJJ, et al. IL-12p40/IL-23p40 blockade with ustekinumab decreases the synovial inflammatory infiltrate through modulation of multiple signaling pathways including MAPK-ERK and Wnt. *Front Immunol.* 2021;12:611656. doi:10.3389/fimmu.2021.611656
50. Pescador N, Francisco V, Vázquez P, et al. Metformin reduces macrophage HIF1 α -dependent proinflammatory signaling to restore brown adipocyte function in vitro. *Redox Biol.* 2021;48:102171. doi:10.1016/j.redox.2021.102171
51. Michael H, Giovanni A, Thomas E, et al. Best practice in research – overcoming common challenges in phytopharmacological research. *J Ethnopharmacol.* 2019;246:112230. doi:10.1016/j.jep.2019.112230

Drug Design, Development and Therapy

Dovepress

Publish your work in this journal

Drug Design, Development and Therapy is an international, peer-reviewed open-access journal that spans the spectrum of drug design and development through to clinical applications. Clinical outcomes, patient safety, and programs for the development and effective, safe, and sustained use of medicines are a feature of the journal, which has also been accepted for indexing on PubMed Central. The manuscript management system is completely online and includes a very quick and fair peer-review system, which is all easy to use. Visit <http://www.dovepress.com/testimonials.php> to read real quotes from published authors.

Submit your manuscript here: <https://www.dovepress.com/drug-design-development-and-therapy-journal>